Activity-dependent tuning of intrinsic excitability in mouse and human neurogliaform cells

Chittajallu, R., Auville, K., Mahadevan, V., Lai, M., Hunt, S., Calvigioni, D., Pelkey, K.A., Zaghloul, K[1]. and McBain, C.J.

Section on Cellular and Synaptic Physiology, *Eunice Kennedy Shriver* National Institute of Child Health and Human Development, National Institutes of Health, Bethesda, MD 20892, USA; [1]Surgical Neurology Branch, National Institutes of Neurological Disorders and Stroke, National Institutes of Health, Bethesda, MD 20892, USA.

ABSTRACT

Spatiotemporal interactions between glutamatergic excitatory and GABAergic inhibitory neurons underly input-output transformations critical for complex brain functions. However, the extent of malleability in this interplay particularly that occuring via modifications in GABAergic interneuron recruitment and output is relatively unexplored in humans. We demonstrate that a specialized interneuron subtype collectively termed neurogliaform cells embedded in both mouse and human neural circuits are susceptible to remarkably similar activity-dependent modulation in their intrinsic properties including the previously characterized distal axonal phenomenon known as barrage firing. Interestingly, we reveal a parallel yet hitherto undescribed plasticity, occurring in the absence of barrage firing manifesting as an enhanced efficacy of excitatory depolarizing inputs to somatodendritic domains in eliciting action potential output. In principle, these evolutionary conserved plasticity routes tune the extent of inhibition mediated by neurogliaform cells constituting circuit mechanisms relevant for human cognitive processing and behavior.

INTRODUCTION

Although heavily outnumbered by glutamatergic pyramidal cells, the population of diverse GABAergic interneuron (INs) subtypes encompass essential components of cortico-hippocampal circuits within the brain[1, 2]. Appropriate interaction between these broad groups of neurons dictates the overall excitation/inhibition balance critical for normal brain function and its protracted dysregulation precipitating neurological disorders. The dynamic nature and capacity of this interplay to undergo modifications in the face of ongoing activity is vital for the correct wiring of cortical circuitry where it is of importance for homeostasis and cognitive tasks such as learning and memory[3, 4, 5, 6, 7, 8]

Since the original theoretical postulations by Hebb and early experimental descriptions[9, 10], a substantial research effort over many decades has uncovered a bewildering array of pathways/mechanisms for the induction and expression of circuit plasticity[8, 11, 12]. The vast majority of our knowledge concerning the varied routes of plasticity expressed by neuronal subtypes is indebted to animal models. However, the extent to which these mechanisms are paralleled in the human central nervous system remain relatively understudied[13]. In particular, the absence of information regarding short- or long-term modulation of excitatory recruitment onto and output of human INs is striking[14, 15].

Successful translation of basic science research conducted in experimental animal models to the clinical setting depends on an integrated knowledge of the similarities and differences in physiological and synaptic properties of neurons in human circuits. In recent years there has been a growing drive and appreciation for such comparisons at the molecular, cellular and physiological levels across evolution[16, 17, 18, 19, 20, 21 22, 23, 24, 25, 26, 27]. We take advantage in availability of human cortical tissue surgically resected for treatment of patients with drug resistant epilepsy. In every participant, our slice electrophysiological analyses were derived from cortical specimens that lay outside of the seizure onset zone as determined by intracranial recordings and thus deemed electrographically normal (see Methods for details). We focus on neurogliaform cells (NGFCs) that together form a large subset of INs that impart inhibition on distal dendritic domains of cortical and hippocampal pyramidal cells [28, 29]. Additionally, NGFCs possess the ability to influence other IN subtypes including each other via chemical (GABA mediated) and electrical (gap junction mediated) modalities[17, 30, 31, 32, 33, 34, 35]. Interestingly, NGFC physiology has been studied not

only in rodents but also in non-human primates and humans revealing both similar and divergent properties across these species[17, 24, 30, 36, 37]. However, only a few reports have described short and long-term plasticity impacting recruitment and activity of mouse NGFCs[38, 39] with a conspicuous lack of published evidence demonstrating any such mechanisms in their human counterparts[15].

In the current study we demonstrate that adult mouse and human NGFCs can undergo analogous forms of activity-dependent modulation of their intrinsic properties. In particular, we reveal a previously undescribed plasticity manifesting as a short-term enhancement in the ability of depolarizing inputs to evoke action potential output which, in mouse, is in part due to functional regulation of subthreshold, transient K^+-conductance(s) (including those mediated by Kv4-containing channels). Although the underlying induction and expression mechanisms remain to be fully determined, this evolutionary retention demonstrates that the ability to modulate NGFC excitability represents canonical mechanisms stressing their importance. From a research perspective, this conservation also highlights the relevance of the mouse model as a predictive tool in basic science research aimed at further unravelling the behavioral correlates dependent on the tuning of NGFC mediated inhibition[40] under physiological and pathological contexts in humans.

RESULTS

Activity-dependent enhancement in intrinsic excitability of NGFCs manifested by barrage firing is evolutionary conserved.

EGFP+ interneurons (INs) with soma located in the superficial portion of *stratum lacunosum-moleculare* (SLM) of mid-ventral hippocampi and Layer I (LI) of cortex (lateral to mid-ventral hippocampi) interneurons in P35-P60 *GAD65*-EGFP or *Htr3A*-EGFP mice were targeted[41, 42, 43]. Using the approach outlined above our data was restricted to NGFCs derived from progenitors located in the caudal ganglionic eminence (i.e. CGE-NGFCs)[29]. Approximately 80% of targeted CGE-NGFCs (124 out of 150 EGFP+ INs) displayed late-spiking (LS; with varying degrees of latency) phenotype and an axo-dendritic morphology characteristic of NGFCs[29](**Fig. 1A;** see **Supplementary Fig. 1** for confocal images of biocytin fills from which reconstructions were drawn). Using brief (2ms) supra-threshold depolarizing current injection steps (1000-1200pA) we elicited 10 action potentials at a frequency of 30Hz repeated at

1 second intervals (**Fig. 1B**). These conditioning APs resulted in the previously described phenomenon of barrage/persistent firing (BF)[15, 44, 45, 46, 47, 48, 49, 50] in approximately 70% of NGFCs tested (86 out of 124 NGFCs; **Fig. 1B Supplementary Fig. 1**). BF constitutes a specific mode of intrinsic plasticity and is characterized by spontaneously generated action potential output in the absence of a depolarizing stimulus. In parallel, INs with soma located in layer I (LI) slices of human cortical tissue (resected from patients with pharmaco-resistant epilepsy in order to gain access to remove the hippocampus, deemed the focal pathological region; see methods for details) were also targeted with a subpopulation demonstrating a late-spiking pattern and morphology identifying them as NGFCs (**Fig 1C**). Upon delivering the same induction protocol as described above, BF was elicited in 48% of human NGFCs (12/25 NGFCs tested; **Fig. 1D; Supplementary Fig. 1**). Interestingly, even with the number of conditioning APs far exceeding that required to induce BF in NGFCs (800 - 1500 APs; 30Hz), BF could not be elicited in superficial cortico-hippocampal INs that were not NGFCs (non-NGFCs), including the recently described human rosehip cell[17] (26 and 37 non-NGFCs tested for BF induction in mouse and human, respectively; **Supplementary Fig. 1**). We tested induction protocols consisting of differing frequencies (8Hz and 100Hz) and these were also found to elicit BF with essentially similar induction requirement and duration **(Fig. 1E,F**). Despite a similar number of conditioning APs necessary for BF induction being similar in both species, the mean BF duration in human NGFCs albeit more variable, was approximately double on average (**Fig. 1E,F**). In some recordings, the induction protocol was continued immediately following cessation of BF to ascertain whether subsequent BF epochs of a longer duration could be triggered. However, NGFCs could not display another bout of BF using this experimental approach (**Supplementary Fig. 2**). Interestingly, subsequent BF episodes could be elicited provided a sufficient refactory period had elapsed between delivery of subsequent induction protocols (**Supplementary Fig. 2**). Circumventing such constraints in BF induction (i.e. allowing greater than 1 minute before subsequent induction delivery) multiple BF episodes (upto four were tested) could be reliably triggered (**Supplementary Fig. 2)**.

Spiking events during NGFC BF episodes in mouse and human were comprised of both spikelets and overshooting action potentials spikes (the latter defined as those in which the peak overshot 0mV; **Figure 1B,D,G**). The spikelet waveform was typically nested within that of the spike as evidenced by a

prominent inflection point in the voltage rise of the latter and in corresponding phase plots (**Fig. 1G,H**). This biphasic rise, noted in previous studies[47, 49], has led to the notion that BF consists of spontaneous AP originating at very distal axonal site(s) that travel retrogradely towards the soma and in some instances subsequently trigger an AP at more proximal sites[47, 49, 50] (hence also referred to as retroaxonal BF[51]). Taken together, these data demonstrate that, of the IN subtypes residing in superficial lamina of cortical and hippocampal microcircuits, NGFCs are privileged with regard an ability to express BF in brief, repeatable episodes. Furthermore, this activity-dependent functional plasticity originating in the distal axonal compartments, is clearly conserved in NGFCs embedded in human cortical circuits.

Potentiation of responses to proximal depolarization in mouse and human NGFCs

During routine monitoring of recording stability before and after BF induction we noted that small depolarizations at the soma employed in voltage clamp to measure access resistance were, in some cases, sufficient to activate action currents after cessation of BF. To investigate further, action potential output to depolarizations via a series of 1s positive current injections before and after BF induction was examined (0 pA to 225 pA; 25 pA steps; **Fig. 2A**). A leftward shift in the input/output curve and increased total number of action potentials were evident after excursions into the BF mode (**Fig. 2B-C**). To ascertain the duration of the observed increased excitability, we reverted to voltage-clamp for more precise control of both the holding membrane potential and the depolarizing stimulus. Action currents in a given NGFC were monitored over time following BF cessation in response to a constant test depolarizing voltage command that was found to be ineffective in eliciting any action currents prior to BF induction (+30mV from a holding potential of -70 mV; **Fig. 2D,E**). Using this approach, the potentiated NGFC output following cessation of BF1 was found to persist for a mean duration of approximately 60 seconds (**Fig. 2F**). Interestingly, even though the duration of BFs expressed in individual NGFCs does not increase with repeated induction (**Supplementary Figure 2**), the potentiation of somatic depolarization-induced output after the cessation of these subsequent BF episodes was markedly prolonged thus demonstrating the ability to prime this mode of plasticity by multiple rounds of induction (**Fig. 2G;** Note: in 3 instances after cessation of BF4 heightened action potential output lasted 900 seconds at which point the experiment was terminated). Thus, in addition to the ability to undergo brief periods of distal axonal plasticity (i.e BF),

both mouse and human NGFCs also exhibit an activity-dependent increase in the sensitivity to proximal somatic depolarizing stimuli. Like BF, this phenomenon is restricted to NGFCs and for the remainder of the manuscript this mode of plasticity will be termed short-term potentiation of somatic-depolarization driven excitability (STP-SE).

Relatively modest activity induces STP-SE independently of BF in both mouse and human NGFCs

Short periods of BF generated in distal axonal region(s) with subsequent driving of action potentials that likely back-propagate into the dendritic tree[39] could conceivably trigger modulatory pathways to influence intrinsic excitability resulting in STP-SE. Therefore, we sought to determine whether BF expression is a prerequisite for STP-SE by employing a protocol designed to assay the minimum induction requirements for the latter form of plasticity. This was achieved by eliciting action potential spiking in response to test rheobase current injection steps of 250 to 300 ms length via the patch pipette (typically 200pA). After a baseline period, an induction paradigm was initiated by delivery of conditioning APs as previously described (10 action potentials at 30Hz) while monitoring action potential output to the same test current pulse (**Figure 3A**). The induction protocol was maintained until commencement of a gradual loss of delay to spiking was noted at which point the conditioning APs were terminated and action potential output to the rheobase current injection continued to be assayed (**Figure 3A**). Notably, with this induction strategy, STP-SE was readily elicited in the absence of measurable BF in mouse (n-9) and human NGFCs (n-4; **Figure 3A-C**) with the mean number of conditioning APs to elicit potentiation in excitability significantly lower than that required to induce BF (**Figure 3D**). As with BF, a subset of NGFCs (7/16 and 2/6 mouse and human NGFCs, respectively) and non-late spiking INs (4/4 and 3/3 mouse and human non-NGFCs, respectively) were unable to undergo STP-SE even under protracted period of conditioning APs (**Figure 3D; Supplementary Figure 3**). Finally, this potentiation of intrinsic excitability was characterized by a significant hyperpolarization of action potential threshold (**Figure 3F-H**) and reduction in the delay to spiking (**Figure 3B,C, I**) which in combination likely contributes to STP-SE. Together, these data demonstrate the propensity of both mouse and human NGFCs to undergo an activity-dependent potentiation of their action potential output in response to somatic depolarizations without the requirement of entering into BF. Moreover, the remarkable

conservation of this intrinsic plasticity from mouse to human NGFCs validates the utility and relevance of the animal model to further investigate the underlying mechanisms. For the remainder of the study, we confine our analyses to mouse hippocampal NGFCs to permit a detail insight into the underlying cellular underpinnings for STP-SE expression.

A Transient K^+-conductance controls intrinsic excitability of mouse NGFCs

Numerous cellular conductances operating at subthreshold voltages, including those carried by K^+-channels, are well suited to influence both the delay to spiking and action potential threshold in a variety of neuronal subtypes. Thus, dynamic modulation of their function constitutes a potentially rapid and powerful cellular mechanism to modulate intrinsic excitability. However, little is known about the complement of K^+-channels in positively identified NGFCs[29]. Under conditions of voltage-gated Na^+- and low threshold Ca^{2+}-channel block, a depolarizing ramp, indicative of an NGFC identity, is clearly apparent in a subpopulation of *Htr3A*-EGFP SLM interneurons in response to somatic current injections (**Figure 4A**). Restricting our analyses to this subset of recorded neurons, standard voltage-clamp protocols in combination with a pharmacological approach were performed to investigate K^+-channel expression. Depolarizing steps from -70 mV to membrane potentials close to AP threshold (AP threshold in NGFCs = -29 ± 0.3 mV; n=70 ; **Figure 4B,C)** revealed both inactivating and to a lesser extent sustained K^+-conductances operating at subthreshold membrane potentials in NGFCs were clearly present (**Figure 4B,C**). Activity of subthreshold Kv1 conductances, in particular Kv1.1 (often referred to as D-type) have been linked to the phenomenon of both late-spiking and action potential threshold in excitatory and inhibitory neuronal subtypes[52, 53, 54, 55]. However, the subthreshold K^+-conductance(s) in NGFCs was not significantly inhibited by α-dendrotoxin (DTX; 100-200nM), a specific blocker of Kv1 (Kv1.1, Kv1,2 and Kv1.6) channels (**Figure 4D**). A low concentration of 4-AP (low 4-AP; 100μM), which also blocks Kv1 channels, caused only a modest yet statistically significant inhibition of subthreshold K^+-conductance(s) (**Figure 4D**). In contrast, millimolar concentrations of 4-AP (high 4-AP; 1-3mM) produced a significant robust inhibition of the subthreshold K^+-conductance with this digitally-isolated conductance exhibiting a distinct inactivating time profile reminiscent of A-type K^+-channels (I_{KA}; **Figure 4D,E**). We next examined the extent to which these pharmacological manipulations affected delay to spike and action potential

threshold. Although DTX and low 4-AP reduced the delay to spike and hyperpolarized action potential threshold, the extent to which this occurs was quite variable and not as marked to that seen following induction of STP-SE (**Figure 4F,I**). In contrast, high 4-AP and 4-AP delivered to NGFCs via the intracellular patch pipette (intra 4-AP; 3mM)[46], modulated the delay to spike and hyperpolarized the AP threshold to an extent that more closely mimics the shift in both these parameters observed during STP-SE (**Figure 4G-I**).

Next, the ability of these pharmacological manipulations to increase intrinsic excitability in response to suprathreshold somatic current injections (1.5 × rheobase) was analyzed. In agreement with the propensity to modulate spike latency and AP threshold (**Figure 4I**) DTX and low 4-AP increased intrinsic excitability to a much lesser extent than high 4-AP or intra 4-AP (**Figure 5A-C**). Interestingly (in the presence of TTX) pharmacological inhibition of I_{KA} with millimolar concentrations of 4-AP results in a transformation of the membrane voltage response characterized by the emergence of a depolarizing hump (**Figure 5D**) as would be predicted by the time-dependent profile of I_{KA} (**Figure 4B,E**). This increased envelope of depolarization, particularly at the onset of the depolarizing stimulus step, must contribute to the loss of delay to spike and increased excitability seen during STP-SE (**Figures 2A,3B 4G-I**).

We next took advantage of a characteristic biophysical property of I_{KA} that manifests as a temporal delay in recovery of activation following inactivation to further investigate its role in NGFCs. Thus, by delivering depolarizing subthreshold pulses in quick succession the extent of I_{KA} influence in NGFCs could be experimentally “titrated” (**Figure 5E,G**). In a separate series of experiments, we assessed the spike delay under conditions where the extent of I_{KA} activation was manipulated in this manner (**Figure 5F,G**). We reveal that the time course of the recovery from inactivation of I_{KA} is mirrored by that seen in the recovery of the delay to spike (**Figure 5G**). Furthermore, a close relationship exists between the extent of I_{KA} inhibition in NGFCs (mediated by the differing magnitudes of recovery from inactivation) and corresponding increase in intrinsic excitability as measured by action potential output to the depolarizing test current injection (**Figure 5H**). Together, these pharmacological/biophysical analyses demonstrate that a transient, subthreshold K^+-conductance(s) sensitive to high concentrations of 4-AP is

a major contributor in dictating action potential latency, threshold and ultimately intrinsic excitability in NGFCs.

We next examined the extent to which pharmacological block of the I_{KA} alters the ability of NGFCs to express STP-SE. For these experiments, I_{KA} was blocked by introduction of 4-AP via the recording pippete as previously described (**Figure 4H; Figure 5A**) to prevent circuit wide perturbations that could confound the interpretation of results[45]. Interleaved experiments (K-gluconate control vs. K-gluconate with intra 4-AP) clearly demonstrate that STP-SE could be induced more readily 4-AP containing internal solution as indicated by a leftward shift in the time course of potentiation that corresponds to a significant reduction in the number of required conditioning APs (**Figure 5I,J**). This gain of function provides further evidence for a reduction in function of 4-AP sensitive conductance(s) in particular those that resemble I_{KA}, as a contributing factor in STP-SE. However, due to our inability to fully occlude STP-SE we cannot fully rule out a role for additional modulation of other channels that are insensitive to intra-4-AP block.

Functional I_{KA} in mouse NGFCs is primarily mediated by Kv4 subunit containing channels

K^+-channels comprised of distinct subunits can contribute to I_{KA} in neural cell types [56]. Channels containing alpha subunits Kv1.1 (when in combination certain auxiliary subunits e.g. Kvβ1), Kv1.4, Kv3.3, Kv3.4 and Kv4 subunits can all mediate I_{KA} and regulate neuronal excitability[56, 57]. The complement of channels responsible for this conductance in NGFCs, however, has not been previously explored. Our previous pharmacological analyses to this point (**Figure 4**) suggest a relatively small contribution of Kv1.1 in increasing intrinsic excitability of NGFCs that in itself is not sufficient to fully recapitulate the changes observed in STP-SE(**Figure 5B**) thus implicating additional transient K^+-channels. As a first pass to identify the molecular identity of I_{KA} in NGFCs, we probed the publicly available Allen Brain Institute mouse dataset[58] (https://portal.brain-map.org/atlases-and-data/rnaseq#Mouse_Cortex_and_Hip; see methods for details) containing single-neuron mRNA profiles of ~76,000 pan-glutamatergic and pan-GABAergic corticohippocampal neurons. Applying unsupervised graph-based clustering approaches using Seurat v3[59, 60], we observed the cardinal neuronal classes (**Supplementary Figure 4A,B),** including a clear segregation of the MGE and CGE-derived GABAergic interneurons. Focusing attention on the

3626 neurons within the cluster corresponding to corticohippocampal CGE-NGFCs (**Figure 6B; Supplementary Figure 4C;** see methods for details) these analyses reveal that essentially no mRNA encoding for Kv1.4 (*KCNA4*), Kv3.3 (*KCNC3*) and Kv4.1 (*KCND1*) subunits indicating their unlikely contribution to I_{KA} in CGE-NGFCs (**Figure 6B**). In contrast, appreciable mRNA levels of *KCNC4*, *KCND2* and *KCND3* mRNA that encode for Kv3.4, Kv4.2 and Kv4.3 subunits, respectively, were apparent (**Figure 6B**). We employed standard voltage-step protocols and digital subtraction to isolate sustained (I_{KDR}) and I_{KA} currents in mouse hippocampal NGFCS (**Figure 6B**) to determine the relative contributions of these subunits in mediating I_{KA} in NGFCs. As expected, TEA at the concentrations used (2 -10 mM) reliably inhibits I_{KDR} (**Figure 6C,D**). However, I_{KA} in NGFCs is TEA insensitive indicating that Kv3.4 does not appreciably mediate NGFC I_{KA}[61] despite the presence of detectable levels of mRNA (**Figure 6C,D**). In contrast, I_{KA} is largely abolished by the selective Kv4 blocker, AmmTx3[62] (% baseline I_{KA} peak after 200nM AmmTx3 = 29.6 ± 9.9 %; n=4; **Figure 6C,D**). Since the expression and functional role of Kv4-channels and their associated auxiliary subunits have been well characterized in principal cells, particularly those of the hippocampus[63], we compared mRNA expression in in these principal cells to that seen in CGE-NGFCs. In general, KCND2/Kv4.2 is predominantly expressed in PCs, particularly those in the CA1 region (**Figure 6E,F;** see methods for details), whereas KCND3/Kv4.3 is mainly restricted to INs[64, 65, 66, 67]. Here, the molecular profile analyses demonstrate that at least at the transcript level as revealed by RNAseq analyses, NGFCs possess comparable levels of combined mRNA encoding KCND2 and KCND3 to that seen in PCs (**Figure 6E**). In agreement with the RNAseq and functional data, *in situ* hybridization using the RNAscope platform revealed the presence of detectable KCND2 and KCND3 mRNA in putative SLM hippocampal NGFCs (identified by NDNF mRNA expression; **Figure 6G,H**). Finally, expression of mRNA for well-known Kv4 auxiliary subunits KCHIPs and DPLPs in NGFCs (particularly KCNIP1, KCNIP4, DPP6 and DPP10) albeit with a differential complement, is essentially similar if not higher to that observed in hippocampal pyramidal cells (**Figure 6I-K**). Interestingly, the presence of DPP6 or DPP10 in the macromolecular complex of Kv4 channels is a requirement in conferring high AmmTx3 sensitivity[62]. Taken together the combined molecular, physiological and pharmacological approach demonstrate that the majority of mouse hippocampal CGE-NGFC I_{KA} which

strongly influences intrinsic excitability of this IN subtype, is most likely mediated via Kv4.1 and Kv4.2 containing channels.

Modulation of dendritic integration by Kv4 channels and activity-dependent potentiation of E-S coupling in mouse NGFCs.

Kv4 containing channels are located along the somatodendritic axis of neurons and influence membrane voltage responses to incoming inputs impinging on these subcellular domains. Therefore, we evaluated their potential role on the dendritic integration of EPSPs elicited in NGFCs. Electrical stimulation of SLM afferents elicited excitatory input onto NGFCs that displayed paired pulse facilitation in agreement with previous observations[35, 38, 41](**Figure 7A**). Bath application of AmmTx3 had no significant effect on either the amplitude of EPSCs nor their paired pulse ratio, whereas a marked significant increase in the depolarization elicited by the same EPSCs when monitored as EPSPs in current clamp (**Figure 7A-D**). These data demonstrate that pharmacological modulation of Kv4 mediated I_{KA} conductance in NGFCs alone, produces EPSP amplification markedly increasing temporal summation of excitatory afferent inputs onto NGFCs, independent to any changes in presynaptic release probability or postsynaptic glutamate receptor function. To this point in our study, we have assayed intrinsic excitability only in response to “artificial” depolarizing current injection steps delivered to the soma. Based on our data thus far we would predict that if STP-SE occurs partly from a reduction of somatodendritic I_{KA}, an increase E-S coupling would be one physiological manifestation. Therefore, in a final set of experiments we probed the effect STP-SE on the integration of synaptic inputs onto NGFCs. EPSPs were evoked in NGFCs by electrical stimulation of SLM afferent fibers (**Figure 7E**). The NGFCs were then exposed to the induction protocol as previously described (**Figure 3A,B**) which was terminated immediately upon expression of STP-SE (**Figure 7F**). Electrical stimulation was recommenced at the same intensity as that used during baseline. In 10 out of 17 NGFCs tested, an increase in action potential output in response to synaptically evoked EPSPs was clearly evident (**Figure 7G,H**). This potentiation of EPSP-spike (E-S) coupling possessed a similar mean duration to that seen in increased intrinsic excitability upon somatic depolarization following a single round of conditioning APs indicating similar underlying mechanisms (**Figure 7H vs. Figure 2G;** 63 ± 11 s vs. 77± 23 s for duration of STP-SE and E-S coupling potentiation,

respectively; n = 10, 37; p = 0.9; Mann-Whitney U -Test). In most recordings a biased current was imposed to ensure resting membrane voltage was equivalent between baseline and post STP-SE induction (Vm = -63.0 ± 0.7 mV vs. -62.7 ± 0.9 mV for baseline and post-induction, respectively; n=10; p = 0.52, Mann-Whitney U-Test). It must be noted that in these experiments, synaptic parameters such as probability of release and postsynaptic receptor function could potentially influence the extent of E-S coupling. Therefore, we also interrogated spontaneous EPSC parameters following induction of multiple BF episodes that have been shown to robustly condition the expression of STP-SE (**Figure 2G**). Interestingly, a small but significant decrease in sEPSC amplitude after the 4th BF episode (post-BF4) was noted, however, this would in fact *negatively* impact any potentiation noted and serve to minimize heightened E-S coupling. In addition, no significant changes in sEPSC frequency nor tau decay were observed (**Supplementary Figure 5**). Together analyses of spontaneous EPSCs following induction of STP-SE confirm a modulation of intrinsic properties as the main underlying cause for the increased E-S coupling observed. In sum, our combined data demonstrate that modulation of I_{KA} in NGFCs (that is mainly mediated by Kv4- containing channels) can effectively influence dendritic integration of excitatory afferent input pointing to a contributing role in the enhanced E-S coupling noted during STP-SE. However, we cannot fully exclude additional contributions by other channels expressed along the axodendritic axes (e.g. KCNQ, HCN, ether-a-go-go, SK/BK channels), a complex interplay of which could contribute to produce the enhanced excitability and E-S coupling described here.

DISCUSSION

Varying mouse IN subtypes, including those in the NGFC family**,** possess the ability to demonstrate barrage or persistent firing[15, 44, 45, 47, 48, 49, 50, 51, 68]. BF is characterized by epochs of action potential output in the absence of depolarizing synaptic input thus circumventing canonical intraneuronal information transfer governed by neuronal polarity. However, induction of barrage firing typically requires protracted periods of action potential activity [44, 47](but see [68, 69]) questioning the exact physiological circumstances under which it manifests. Its operational role in normal brain function therefore remains unclear, although it has been postulated to constitute a mechanism for driving network oscillations[15], an important function of IN subclasses including NGFCs[1, 29, 70]. From a pathological standpoint, it has been

proposed to constitute a homeostatic, dampening mechanism during prolonged epochs of circuit overexcitation such as those that occur during epilepsy[44, 49]. Here we demonstrate the evolutionary retention of this IN subtype to enter this specific mode of intrinsic excitability and future work will be required to determine its exact role in human circuits. In addition to BF, we reveal the existence of a distinct and previously undescribed intrinsic plasticity mechanism expressed by both mouse and human NGFCs characterized by an increased efficacy of depolarizing input to elicit action potential output which we term STP-SE. We propose that, due to its relatively modest activity requirements, STP-SE possesses a greater propensity to operate under more physiological activity regimens. Furthermore, it is envisaged that during the period of STP-SE, NGFCs can exhibit heightened inhibitory influence in response to afferent activity patterns driven by relevant stimuli and ongoing behavior.

Mechanistic studies have highlighted various cellular pathways and downstream molecular targets responsible for shaping intrinsic properties of IN subtypes precipitated by activity and/or following sensory/behavioral modification[49, 53, 71, 72, 73]. With respect to the NGFC subfamily of interneurons, activation of G-protein signaling cascades modulates their intrinsic excitability although the downstream molecular targets remain unclear[45, 48]. In the current study, we show that mouse NGFCs express Kv4 and auxiliary subunit transcripts that translates to a functional I_{KA} conductance. Although the ramifications of Kv4 channel and auxiliary subunits have been mainly investigated in pyramidal cells, their expression and role in modulating subthreshold membrane dynamics, firing properties and dendritic excitability of IN subtypes have been described[1, 65, 67, 72, 74, 75, 76, 77, 78, 79]. We extend these observations to NGFCs and demonstrate I_{KA} can effectively influence delay to spike and action potential threshold resulting in increased intrinsic excitability similar to that seen in STP-SE ultimately resulting in enhanced dendritic integration. This coupled with the fact that STP-SE is more readily induced under conditions where I_{KA} is inhibited points to a potential modulation of this conductance in the expression of intrinsic plasticity described in this study. Phosphorylation of Kv4, including that elicited by PKA, PKC and MAP/ERK activated by G-protein signaling cascades and/or changes in intracellular calcium functionally regulates expression of and the biophysical properties of these channels[80, 81]. Additionally, the existence of marked expression of mRNA encoding for members of the KChIP auxiliary subunits, acting as intracellular calcium sensors, in NGFCs provides an additional mechanism for Kv4 channel modulation[63, 82]. Together,

these possible cellular routes link neuronal activity to the modulation of subthreshold I_{KA} conductances that ultimately dictate NGFC excitability. However, care must be taken in extrapolating mechanistic studies performed in mouse to human especially in light of recent observations highlighting divergence of molecular properties between equivalent IN subtypes across evolution [18, 19]. For example, examination of available RNAseq data from mouse and human via available transcriptomic explorers[18, 19] (https://portal.brain-map.org/; http://interneuron.mccarrolllab.org/) reveals essentially a complete absence of *KCNA1* mRNA levels in human IN populations (**Supplementary Fig. 6**). Indeed, a number of studies have highlighted an important role of Kv1.1 for mouse IN excitability[8, 53, 71, 73], thus these cross-species transcriptomic profiling data questions to what extent its functional modulation is relevant for shaping IN excitability within humans. As previously discussed, Kv1.1 plays a minimal role with a relatively larger and measurable impact of Kv4-channel mediated I_{KA} in dictating mouse NGFC excitability. Interestingly, gene expression of *KCND2*, *KCND3* (and associated auxiliary subunit mRNA; https://portal.brain-map.org/; http://interneuron.mccarrolllab.org/) are conserved across evolution (**Supplementary Fig. 6**). Although further investigation will be required to directly assay the functional roles of these subthreshold conductances, the described gene expression studies point to a maintained presence of Kv4-containing channels highlighting them as potential molecular targets in dictating human NGFC excitability.

At the cellular level, dendritic inhibition exerts a strong influence on excitability and electrogenesis in distal pyramidal cell subdomains[1, 2]. At the network level this translates into changes in efficiency of pyramidal cell recruitment, gating of information transfer within neural circuits, sculpting the propensity for induction/expression of synaptic plasticity and coordinating pyramidal cell ensembles to generate specific oscillatory events that are known to underly cognitive processing. Given these critical network roles, it is not surprising that various behaviors are encoded through the activity and modulation of dendritic targeting INs[83, 84 40]. However, although constituting one of the major populations of INs providing dendritic inhibition[28] limited information is available regarding the *in vivo* role of the NGFC subfamily. Recently, a correlation between the recruitment of inhibition mediated by NDNF-expressing cells (a subpopulation corresponding to NGFCs[40, 85] and conditioned learning in mice has provided the first description of a link between NGFC function and behavior[40]. The control of dendritic excitability, including that mediated by Kv4 channels, alters the propensity for LTP induction/expression of excitatory afferent

input onto pyramidal cells[86]. Interestingly, mouse NGFCs also exhibit Hebbian long-term plasticity (LTP) triggered by Ca^{2+}-influx via NMDA receptor and/or VGCC activation[38]. NGFCs located in superficial regions of cortex and hippocampus are impinged upon via multiple glutamatergic (e.g. thalamic and cortical) and neuromodulatory afferent populations [38, 40, 41, 43] each conveying distinct information. Thus, it is plausible that increased intrinsic excitability occurring in response to the activity of a given specific afferent input can render a second distinct input more efficacious in NGFC recruitment for short- or long-term periods. Together, these outlined metaplastic routes potentially arising from the modulation of intrinsic plasticity described here, including the subsequent gating and influence of synaptic plasticity in excitatory transmission onto pyramidal cells via the modulation of dendritic inhibition, bestows the microcircuit with a complex array of cellular mechanisms relevant for top-down processing and encoding of contextual information underlying specific learning and memory tasks[40].

In the current study, we focused on mouse and human NGFCs that reside in the most superficial regions of cortico-hippocampal circuitry. These NGFCs are largely derived from an embryonic progenitor pool originating in the caudal ganglionic eminence (CGE)[29]. Another distinct group of NGFCs (along with Ivy cells) have been identified particularly in mouse hippocampus and can be delineated based on a distinct developmental origin in the medial ganglionic eminence (MGE). Intriguingly, recent cross-species transcriptomic analyses have revealed a remarkable expansion (in terms of number relative to the other IN subtypes) of MGE-derived NGFCs that appear in deeper layers of human sensory and associational cortices when compared to equivalent brain regions in mouse[19]. Whether this expanded population of MGE-derived cortical NGFC population in humans undergo similar intrinsic property modulation to their CGE counterparts described here remains to be determined. If so, this would markedly increase the available substrate, further expanding the influence of the described plasticity in cortical circuits of humans.

REFERENCES

1. Pelkey KA, Chittajallu R, Craig MT, Tricoire L, Wester JC, McBain CJ. Hippocampal GABAergic Inhibitory Interneurons. *Physiol Rev* **97**, 1619-1747 (2017).

2. Kepecs A, Fishell G. Interneuron cell types are fit to function. *Nature* **505**, 318-326 (2014).

3. Butt SJ, Stacey JA, Teramoto Y, Vagnoni C. A role for GABAergic interneuron diversity in circuit development and plasticity of the neonatal cerebral cortex. *Curr Opin Neurobiol* **43**, 149-155 (2017).

4. Takesian AE, Hensch TK. Balancing plasticity/stability across brain development. *Prog Brain Res* **207**, 3-34 (2013).

5. Tien NW, Kerschensteiner D. Homeostatic plasticity in neural development. *Neural Dev* **13**, 9 (2018).

6. Pozo K, Goda Y. Unraveling mechanisms of homeostatic synaptic plasticity. *Neuron* **66**, 337-351 (2010).

7. Keck T*, et al.* Integrating Hebbian and homeostatic plasticity: the current state of the field and future research directions. *Philos Trans R Soc Lond B Biol Sci* **372**, (2017).

8. Debanne D, Inglebert Y, Russier M. Plasticity of intrinsic neuronal excitability. *Curr Opin Neurobiol* **54**, 73-82 (2019).

9. Hebb DO. *The organization of behavior: A neurophysiological theory*. John Wiley and Sons (1949).

10. Bliss T, Collingridge G. Persistent memories of long-term potentiation and the N-methyl-d-aspartate receptor. *Brain and Neuroscience Advances* **3**, 2398212819848213 (2019).

11. Kullmann DM, Moreau AW, Bakiri Y, Nicholson E. Plasticity of inhibition. *Neuron* **75**, 951-962 (2012).

12. Malenka RC, Bear MF. LTP and LTD: an embarrassment of riches. *Neuron* **44**, 5-21 (2004).

13. Mansvelder HD, Verhoog MB, Goriounova NA. Synaptic plasticity in human cortical circuits: cellular mechanisms of learning and memory in the human brain? *Curr Opin Neurobiol* **54**, 186-193 (2019).

14. Szegedi V*, et al.* Plasticity in Single Axon Glutamatergic Connection to GABAergic Interneurons Regulates Complex Events in the Human Neocortex. *PLoS Biol* **14**, e2000237 (2016).

15. Rózsa M, Toth M, Olah G, Baka J, Barzo P, Tamas G. Rhythmic persistent firing of neurogliaform interneurons in the human and rodent neocortex.) (2017).

16. Beaulieu-Laroche L*, et al.* Enhanced Dendritic Compartmentalization in Human Cortical Neurons. *Cell* **175**, 643-651 e614 (2018).

17. Boldog E*, et al.* Transcriptomic and morphophysiological evidence for a specialized human cortical GABAergic cell type. *Nat Neurosci* **21**, 1185-1195 (2018).

18. Hodge RD*, et al.* Conserved cell types with divergent features in human versus mouse cortex. *Nature* **573**, 61-68 (2019).

19. Krienen FM*, et al.* Innovations in Primate Interneuron Repertoire. *bioRxiv*, (2019).

20. Obermayer J*, et al.* Lateral inhibition by Martinotti interneurons is facilitated by cholinergic inputs in human and mouse neocortex. *Nat Commun* **9**, 4101 (2018).

21. Szegedi V*, et al.* Robust perisomatic GABAergic self-innervation inhibits basket cells in the human and mouse supragranular neocortex. *Elife* **9**, (2020).

22. Eyal G*, et al.* Unique membrane properties and enhanced signal processing in human neocortical neurons. *Elife* **5**, (2016).

23. Povysheva NV, Zaitsev AV, Rotaru DC, Gonzalez-Burgos G, Lewis DA, Krimer LS. Parvalbumin-positive basket interneurons in monkey and rat prefrontal cortex. *J Neurophysiol* **100**, 2348-2360 (2008).

24. Poorthuis RB*, et al.* Rapid Neuromodulation of Layer 1 Interneurons in Human Neocortex. *Cell Rep* **23**, 951-958 (2018).

25. Molnar G*, et al.* Human pyramidal to interneuron synapses are mediated by multi-vesicular release and multiple docked vesicles. *Elife* **5**, (2016).

26. Szabadics J, Varga C, Molnar G, Olah S, Barzo P, Tamas G. Excitatory effect of GABAergic axo-axonic cells in cortical microcircuits. *Science* **311**, 233-235 (2006).

27. Varga C, Tamas G, Barzo P, Olah S, Somogyi P. Molecular and Electrophysiological Characterization of GABAergic Interneurons Expressing the Transcription Factor COUP-TFII in the Adult Human Temporal Cortex. *Cereb Cortex* **25**, 4430-4449 (2015).

28. Bezaire MJ, Soltesz I. Quantitative assessment of CA1 local circuits: knowledge base for interneuron-pyramidal cell connectivity. *Hippocampus* **23**, 751-785 (2013).

29. Overstreet-Wadiche L, McBain CJ. Neurogliaform cells in cortical circuits. *Nat Rev Neurosci* **16**, 458-468 (2015).

30. Olah S*, et al.* Output of neurogliaform cells to various neuron types in the human and rat cerebral cortex. *Front Neural Circuits* **1**, 4 (2007).

31. Armstrong C, Szabadics J, Tamas G, Soltesz I. Neurogliaform cells in the molecular layer of the dentate gyrus as feed-forward gamma-aminobutyric acidergic modulators of entorhinal-hippocampal interplay. *J Comp Neurol* **519**, 1476-1491 (2011).

32. Chittajallu R, Pelkey KA, McBain CJ. Neurogliaform cells dynamically regulate somatosensory integration via synapse-specific modulation. *Nat Neurosci* **16**, 13-15 (2013).

33. Chu Z, Galarreta M, Hestrin S. Synaptic interactions of late-spiking neocortical neurons in layer 1. *J Neurosci* **23**, 96-102 (2003).

34. Simon A, Olah S, Molnar G, Szabadics J, Tamas G. Gap-junctional coupling between neurogliaform cells and various interneuron types in the neocortex. *J Neurosci* **25**, 6278-6285 (2005).

35. Price CJ*, et al.* Neurogliaform neurons form a novel inhibitory network in the hippocampal CA1 area. *J Neurosci* **25**, 6775-6786 (2005).

36. Povysheva NV*, et al.* Electrophysiological differences between neurogliaform cells from monkey and rat prefrontal cortex. *J Neurophysiol* **97**, 1030-1039 (2007).

37. Zaitsev AV*, et al.* Interneuron diversity in layers 2-3 of monkey prefrontal cortex. *Cereb Cortex* **19**, 1597-1615 (2009).

38. Mercier MS, Magloire V, Cornford JH, Kullmann DM. Long-term synaptic plasticity in hippocampal neurogliaform interneurons. *bioRxiv*, (2019).

39. Li G, Stewart R, Canepari M, Capogna M. Firing of hippocampal neurogliaform cells induces suppression of synaptic inhibition. *J Neurosci* **34**, 1280-1292 (2014).

40. Abs E*, et al.* Learning-Related Plasticity in Dendrite-Targeting Layer 1 Interneurons. *Neuron* **100**, 684-699 e686 (2018).

41. Chittajallu R*, et al.* Afferent specific role of NMDA receptors for the circuit integration of hippocampal neurogliaform cells. *Nat Commun* **8**, 152 (2017).

42. Tricoire L, Pelkey KA, Erkkila BE, Jeffries BW, Yuan X, McBain CJ. A blueprint for the spatiotemporal origins of mouse hippocampal interneuron diversity. *J Neurosci* **31**, 10948-10970 (2011).

43. Lee S, Hjerling-Leffler J, Zagha E, Fishell G, Rudy B. The largest group of superficial neocortical GABAergic interneurons expresses ionotropic serotonin receptors. *J Neurosci* **30**, 16796-16808 (2010).

44. Suzuki N, Tang CS, Bekkers JM. Persistent barrage firing in cortical interneurons can be induced in vivo and may be important for the suppression of epileptiform activity. *Front Cell Neurosci* **8**, 76 (2014).

45. Deemyad T, Luthi J, Spruston N. Astrocytes integrate and drive action potential firing in inhibitory subnetworks. *Nat Commun* **9**, 4336 (2018).

46. Jung SC, Hoffman DA. Biphasic somatic A-type K channel downregulation mediates intrinsic plasticity in hippocampal CA1 pyramidal neurons. *PLoS One* **4**, e6549 (2009).

47. Sheffield ME, Best TK, Mensh BD, Kath WL, Spruston N. Slow integration leads to persistent action potential firing in distal axons of coupled interneurons. *Nat Neurosci* **14**, 200-207 (2011).

48. Krook-Magnuson E, Luu L, Lee SH, Varga C, Soltesz I. Ivy and neurogliaform interneurons are a major target of mu-opioid receptor modulation. *J Neurosci* **31**, 14861-14870 (2011).

49. Elgueta C, Kohler J, Bartos M. Persistent discharges in dentate gyrus perisoma-inhibiting interneurons require hyperpolarization-activated cyclic nucleotide-gated channel activation. *J Neurosci* **35**, 4131-4139 (2015).

50. Imbrosci B, Neitz A, Mittmann T. Physiological properties of supragranular cortical inhibitory interneurons expressing retrograde persistent firing. *Neural Plast* **2015**, 608141 (2015).

51. Sheffield ME, Edgerton GB, Heuermann RJ, Deemyad T, Mensh BD, Spruston N. Mechanisms of retroaxonal barrage firing in hippocampal interneurons. *J Physiol* **591**, 4793-4805 (2013).

52. Storm JF. Temporal integration by a slowly inactivating K+ current in hippocampal neurons. *Nature* **336**, 379-381 (1988).

53. Campanac E, Gasselin C, Baude A, Rama S, Ankri N, Debanne D. Enhanced intrinsic excitability in basket cells maintains excitatory-inhibitory balance in hippocampal circuits. *Neuron* **77**, 712-722 (2013).

54. Dehorter N, Ciceri G, Bartolini G, Lim L, del Pino I, Marin O. Tuning of fast-spiking interneuron properties by an activity-dependent transcriptional switch. *Science* **349**, 1216-1220 (2015).

55. Bekkers JM, Delaney AJ. Modulation of excitability by alpha-dendrotoxin-sensitive potassium channels in neocortical pyramidal neurons. *J Neurosci* **21**, 6553-6560 (2001).

56. Rudy B. Diversity and ubiquity of K channels. *Neuroscience* **25**, 729-749 (1988).

57. Carrasquillo Y, Burkhalter A, Nerbonne JM. A-type K+ channels encoded by Kv4.2, Kv4.3 and Kv1.4 differentially regulate intrinsic excitability of cortical pyramidal neurons. *J Physiol* **590**, 3877-3890 (2012).

58. Tasic B*, et al.* Shared and distinct transcriptomic cell types across neocortical areas. *Nature* **563**, 72-78 (2018).

59. Stuart T*, et al.* Comprehensive Integration of Single-Cell Data. *Cell* **177**, 1888-1902.e1821 (2019).

60. Butler A, Hoffman P, Smibert P, Papalexi E, Satija R. Integrating single-cell transcriptomic data across different conditions, technologies, and species. *Nature biotechnology* **36**, 411-420 (2018).

61. Rudy B, McBain CJ. Kv3 channels: voltage-gated K+ channels designed for high-frequency repetitive firing. *Trends Neurosci* **24**, 517-526 (2001).

62. Maffie JK, Dvoretskova E, Bougis PE, Martin-Eauclaire MF, Rudy B. Dipeptidyl-peptidase-like-proteins confer high sensitivity to the scorpion toxin AmmTX3 to Kv4-mediated A-type K+ channels. *J Physiol* **591**, 2419-2427 (2013).

63. Jerng HH, Pfaffinger PJ. Modulatory mechanisms and multiple functions of somatodendritic A-type K (+) channel auxiliary subunits. *Front Cell Neurosci* **8**, 82 (2014).

64. Serodio P, Rudy B. Differential expression of Kv4 K+ channel subunits mediating subthreshold transient K+ (A-type) currents in rat brain. *J Neurophysiol* **79**, 1081-1091 (1998).

65. Lien CC, Martina M, Schultz JH, Ehmke H, Jonas P. Gating, modulation and subunit composition of voltage-gated K(+) channels in dendritic inhibitory interneurones of rat hippocampus. *J Physiol* **538**, 405-419 (2002).

66. Menegola M, Misonou H, Vacher H, Trimmer JS. Dendritic A-type potassium channel subunit expression in CA1 hippocampal interneurons. *Neuroscience* **154**, 953-964 (2008).

67. Rhodes KJ*, et al.* KChIPs and Kv4 alpha subunits as integral components of A-type potassium channels in mammalian brain. *J Neurosci* **24**, 7903-7915 (2004).

68. Wang B*, et al.* A Subtype of Inhibitory Interneuron with Intrinsic Persistent Activity in Human and Monkey Neocortex. *Cell Rep* **10**, 1450-1458 (2015).

69. Yoshida M, Hasselmo ME. Persistent firing supported by an intrinsic cellular mechanism in a component of the head direction system. *J Neurosci* **29**, 4945-4952 (2009).

70. Capogna M. Neurogliaform cells and other interneurons of stratum lacunosum-moleculare gate entorhinal-hippocampal dialogue. *J Physiol* **589**, 1875-1883 (2011).

71. Gainey MA, Aman JW, Feldman DE. Rapid Disinhibition by Adjustment of PV Intrinsic Excitability during Whisker Map Plasticity in Mouse S1. *J Neurosci* **38**, 4749-4761 (2018).

72. Sun QQ. Experience-dependent intrinsic plasticity in interneurons of barrel cortex layer IV. *J Neurophysiol* **102**, 2955-2973 (2009).

73. Li KX*, et al.* Neuregulin 1 regulates excitability of fast-spiking neurons through Kv1.1 and acts in epilepsy. *Nat Neurosci* **15**, 267-273 (2011).

74. Goldberg JH, Tamas G, Yuste R. Ca2+ imaging of mouse neocortical interneurone dendrites: Ia-type K+ channels control action potential backpropagation. *J Physiol* **551**, 49-65 (2003).

75. Wang Y*, et al.* Anatomical, physiological and molecular properties of Martinotti cells in the somatosensory cortex of the juvenile rat. *J Physiol* **561**, 65-90 (2004).

76. Oláh VJ*, et al.* Functional specification of CCK+ interneurons by alternative isoforms of Kv4.3 auxiliary subunits. *bioRxiv*, (2019).

77. Bourdeau ML, Morin F, Laurent CE, Azzi M, Lacaille JC. Kv4.3-mediated A-type K+ currents underlie rhythmic activity in hippocampal interneurons. *J Neurosci* **27**, 1942-1953 (2007).

78. Bourdeau ML, Laplante I, Laurent CE, Lacaille JC. KChIP1 modulation of Kv4.3-mediated A-type K(+) currents and repetitive firing in hippocampal interneurons. *Neuroscience* **176**, 173-187 (2011).

79. Williams SB, Hablitz JJ. Differential modulation of repetitive firing and synchronous network activity in neocortical interneurons by inhibition of A-type K(+) channels and Ih. *Front Cell Neurosci* **9**, 89 (2015).

80. Cerda O, Trimmer JS. Analysis and functional implications of phosphorylation of neuronal voltage-gated potassium channels. *Neurosci Lett* **486**, 60-67 (2010).

81. Debanne D, Russier M. The contribution of ion channels in input-output plasticity. *Neurobiol Learn Mem* **166**, 107095 (2019).

82. Bahring R. Kv channel-interacting proteins as neuronal and non-neuronal calcium sensors. *Channels (Austin)* **12**, 187-200 (2018).

83. Cummings KA, Clem RL. Prefrontal somatostatin interneurons encode fear memory. *Nat Neurosci* **23**, 61-74 (2020).

84. Lovett-Barron M*, et al.* Dendritic inhibition in the hippocampus supports fear learning. *Science* **343**, 857-863 (2014).

85. Tasic B*, et al.* Adult mouse cortical cell taxonomy revealed by single cell transcriptomics. *Nat Neurosci* **19**, 335-346 (2016).

86. Kim J, Hoffman DA. Potassium channels: newly found players in synaptic plasticity. *Neuroscientist* **14**, 276-286 (2008).

87. Mayer C*, et al.* Developmental diversification of cortical inhibitory interneurons. *Nature* **555**, 457-462 (2018).

88. Cembrowski MS, Bachman JL, Wang L, Sugino K, Shields BC, Spruston N. Spatial Gene-Expression Gradients Underlie Prominent Heterogeneity of CA1 Pyramidal Neurons. *Neuron* **89**, 351-368 (2016).

89. Cembrowski MS, Wang L, Sugino K, Shields BC, Spruston N. Hipposeq: a comprehensive RNA-seq database of gene expression in hippocampal principal neurons. *Elife* **5**, e14997 (2016).

Acknowledgments

We thank Apratim Mitra and Ryan Dale at the NICHD Bioinformatics and Scientific Programming Core, and Christopher T. Rhodes for assistance with analyzing the Allen Brain scRNAseq dataset. These analyses utilized the computational resources of the NIH PC Biowulf cluster (http://hpc.nih.gov). We are grateful to Lynne Holtzclaw (NICHD Microscopy and Imaging Core) for invaluable help with tissue preparation, RNAscope and imaging of fluorescent *in situ* hybridization using the RNAscope platform (ACD). We also thank Cameron Paranzino for performing Neurolucida reconstructions of biocytin filled neurons.

Methods

Tissue Procurement

Adult (p35-p60) male and female $5HT_{3A}R$-EGFP or GAD65-EGFP mice were used and all experiments were conducted in accordance with animal protocols approved by the National Institutes of Health (ASP# 17–045). For human data, we collected surgical specimens from ten participants (7 male; age range 22-69 years) with drug-resistant epilepsy who underwent an initial surgical procedure in which intracranial recording electrodes were implanted subdurally on the cortical surface as well as within the brain parenchyma for seizure monitoring followed by a second surgical procedure in which a resection was performed. In each case, the clinical team determined the initial placement of the contacts to localize the epileptogenic zone. Based on the intracranial recordings during the monitoring period, the clinical team then determined which electrode contacts lay over brain regions exhibiting ictal or inter-ictal activity and which contacts were electrographically normal. The surgical resections during the second surgery were designed to remove the areas of seizure onset, but in every case, also involved removal of some brain tissue determined to be electrographically normal. In eight participants, we collected electrographically normal brain specimens from the lateral temporal lobe cortex which was removed as part of a standard anterior temporal lobectomy for resection of the hippocampus. In the two remaining participants, we obtained parietal and frontal lobe brain specimens that were immediately adjacent to the epileptogenic zone but that were also determined to be electrographically normal. The NINDS Institutional Review Board (IRB) approved the research protocol (ClinicalTrials.gov Identifier

NCT01273129), and informed consent for the experimental use of resected tissue was obtained from each participant and their guardians.

Electrophysiology

Both mouse and human brain tissue were sectioned at 300μm using a Leica Vibratome 1200s in ice-cold sucrose-based cutting solution of the following composition (mM): 90 sucrose, 80 NaCl, 3.5 KCl, 24 $NaHCO_3$, 1.25 NaH_2PO_4, 4.5 $MgCl_2$, 0.5 $CaCl_2$, and 10 glucose, saturated with 95% O_2 and 5% CO_2. Slices were allowed to equilibrate in warm (31-33°C) sucrose cutting solution for 20-30 minutes after which the solution was allowed to return to room temperature where they were maintained until electrophysiological analyses. Electrophysiological recordings were performed on slices perfused with extracellular solution of the following composition (mM): 130 NaCl, 24 $NaHCO_3$, 1.25 NaH_2PO_4, 3.5 KCl, 1.5 $MgCl_2$, 2.5 $CaCl_2$ and 10 glucose saturated with 95% O_2 and 5% CO_2. In certain experiments (see results section for details) the extracellular solution was supplemented with one or a combination of the following drugs; 50μM picrotoxin (Millipore Sigma; Cat. No. 80410), 2-5μM CGP556845A (Abcam; Cat. No. ab120337), 5-10μM bicuculline methobromide (Abcam; Cat. No. ab120109), 100μM or 1-3mM 4-aminopyridine (Millipore Sigma; Cat. No. A78403), 100-200nM α -DTX (Alomone Labs; Cat No.D-350), 200 or 500nM AmmTx3 (Alomone Labs; Cat No.STA-305). Whole cell voltage and current-clamp recordings were performed at 32–34 °C with electrodes (3–5MΩ) pulled from borosilicate glass (World Precision Instruments, Sarasota, FL) filled with intracellular solution of the following composition (in mM); 150 K–gluconate, 3 $MgCl_2$, 0.5 EGTA, 2 MgATP, 0.3 Na_2GTP, 10 HEPES and 3 mg/ml biocytin; pH was adjusted to 7.3 with KOH and osmolarity adjusted to 280–300 mOsm. All electrophysiological recordings were performed using Multiclamp 700B amplifier (Molecular Devices, Sunnyvale, CA, USA). Signals were filtered at 4–10 kHz and digitized at 10–20 kHz (Digidata 1322A and pClamp 10.2 Software; Molecular Devices, Sunnyvale, CA, USA). For analyses of K^+-channel currents in NGFCs, voltage clamp recordings were performed in the presence of 0.5μm TTX and 200μM $NiCl_2$ with voltage steps delivered as indicated in the manuscript. Digital leak subtraction was performed online (P/4) to remove capacitance transient and leak currents and series resistance compensation was not performed. Glutamate receptor mediated synaptic responses (EPSCs and EPSPs) were evoked with A360 constant-current stimulus isolator

(World Precision Instruments, Sarasota, FL, USA) and with stimulation electrodes pulled from borosilicate glass filled with aCSF placed in SLM in the presence 50μM picrotoxin, 2-5μM CGP556845A and 5-10μM bicuculline to block GABA receptor mediated responses. In experiments assessing the effect of AmmTX3 on EPSP integrations 5mM QX-314Cl$^-$ was included in the intracellular solution to prevent activation of voltage-gated sodium channels.

For neuron morphology recoveries after electrophysiological recordings, slices were post-fixed in 4% paraformaldehyde in 0.1M phosphate buffer at least overnight followed by fluorescent conjugation to biocytin and confocal images attained using a Zeiss 780 microscope (NICHD Microscopy and Imaging Core) and reconstructions drawn using Neurolucida software (MBF Bioscience, VT).

Fluorescence *in situ* hybridization employing the RNAscope® platform

In this study, two mice aged p35 and p40 were anesthetized with isoflurane and intracardially perfused with 0.1M phosphate buffer, Ph7.4, followed by 4% paraformaldehyde/0.1M phosphate buffer. Brains were removed and post-fixed in 4% paraformaldehyde/0.1M phosphate buffer overnight, then embedded in Tissue-Tek® O.C.T. compound {Sakura Finetek, USA Cat. No 4583} and frozen. 10 – 14 μM horizontal sections containing mid-ventral hippocampus were cut using a Leica CM3050-S cryostat, mounted on microscope slides and stored at -80°C until use. Fluorescent *in situ* hybridization was performed according to the RNAscope® (Advanced Cell Diagnostics USA, Newark, CA) protocol using the Multiplex Fluorescent Reagent Kit v1 (Cat. No 320851). Probes employed were Mm-NDNF (Cat No. 447471-C2), Mm-KCND2 (Cat No. 452581) and Mm-KCND3 (Cat No. 573641). Sections were cover-slipped and confocal images taken using Zeiss 780 microscope (NICHD Microscopy and Imaging Core). Z-stack images were acquired using a 20x/0.8 Plan Apochromat or 40x/1.3 Plan Neofluar objective and were rendered as maximum intensity injections.

Analyses of single cell RNAseq (scRNAseq) transcriptomic data available from the Allen Brain Institute

To analyze the Allen Institute mouse dataset of the single-cell transcriptomes of ~76,000 cells from >20 areas of mouse cortex and hippocampus, we downloaded the transcript.tome/HDF5 file

(https://portal.brain-map.org/atlases-and-data/rnaseq) and subsequently converted into Seurat v3-compatible format based on the instructions provided in the Allen Institute Portal (https://portal.brain-map.org/atlases-and-data/rnaseq/protocols-mouse-cortex-and-hippocampus) and custom scripts in R package. Basic processing and visualization of the scRNA-seq data were performed with the Seurat v3 in R[59, 60]. Briefly, data was preprocessed by removing cells with less than 200 detectable genes and with reads mapping to mitochondrial genes comprising more than 0.05% of total reads. Gene expression counts were then log normalized and the resulting expression matrix was scaled to 10,000 transcripts per cell. Next, the expression values of each gene across all the cells (z-score transformation) were utilized for dimensionality reduction. These were performed using the NormalizeData() and ScaleData() functions in Seurat with default parameters. Next, we identified the top 2000 genes that exhibited high variability across cells and therefore represent unique features of the cell clusters, for downstream analysis using the FindVariableGenes() function, by applying selection.method = "vst" feature. Next, principal component analysis (PCA) was performed, and the top 20 principal components were stored. We clustered the cells using the FindClusters() with a clustering resolution set to 0.6. This approach generated a total of 38 clusters. Using the FindAllMarkers() function at cutoff of genes expressed in 25% of cells, at a logfc.threshold = 0.25, we identified the genes that are expressed in each cluster. For each cell type we used the well-established marker genes that uniquely established the cell identity, as previously described in the literature. Notably, *Snap25* positive clusters were annotated as neurons, and the *Snap25* negative clusters were annotated as non-neurons; among the neurons, *Slc17a7* was indicative of glutamatergic and *Gad1* expression indicative of GABAergic neurons **(Supplementary Figure 4A).** More specifically, the *Gad1* clusters expressing a combination of *Lhx6, Pvalb, Sst, Hapln1* are indicative of MGE-derived GABAergic interneurons, and a combination of *Lhx6*-negative*, Prox1, Vip, Calb2, Cnr1, Hapln1, Ndnf* are indicative of CGE-derived GABAergic interneurons **(Supplementary Figure 4B)**. Relevant for the present study, specific-markers include, but are not limited to: *Gad1*, *Prox1*, *Hapln1, Lamp5, Ndnf,* but *Lhx6* negative, for the CGE-NGFCs[58, 87]; *Slc17a7*, *Wfs1*, *Fibcd1*, *Crym* for the hippocampal pyramidal neurons[88, 89]. The expression of KCN genes and auxiliary subunits were obtained for the above clusters, and the Violin/Split-violin plots were plotted via custom scripts in the R package using ggplot.

Statistics

Each dataset that underwent statistical analyses was first tested for normal distribution using the Shapiro-Wilk test. For data that was deemed normally distributed parametric paired or unpaired t-tests were employed, otherwise Mann-Whitney U-tests or Wilcoxin-sign Rank tests were used. Due to the low n numbers in some human datasets (Figure 2C, n=3; Figures 3H, I, n=4), Shapiro-Wilk or non-parametric tests could not be performed and in these cases we defaulted to parametric Students T-test. In the figure panels statistical significance is denoted as follows; * $p<0.05$, ** $p<0.01$, *** $p<0.001$, ns not significant $p>0.05$. The type of statistical test and exact p-values are indicated in the figure legends where appropriate. n values throughout the manuscript correspond to the number of cells tested and for each set of experiments and are from a minimum of 3 mice and 2 human subjects. Throughout the manuscript figures, data in black/grey and orange were from mouse and human, respectively. In box plots, the data are represented as the median and mean (line and symbol, respectively), the 25th and 75th percentile (bottom and top of the box, respectively), 10th and 90th percentiles (bottom and top of whiskers, respectively). In scatter and line plots all data are expressed as the mean ± s.e.m.

Figure Legends

Figure 1. An evolutionary conserved barrage firing in human NGFCs. A,C. Biocytin reconstruction of mouse (dendrites in black; axon in gray) and human NGFCs (dendrites in black; axon in orange) located in superficial regions of hippocampus (*stratum lacunosum moleculare*; SLM) and cortex (Layer I). **B,D.**

Single example trace showing the induction of barrage firing (BF) in mouse and human NGFCs upon delivery of action potentials via 1ms depolarizing steps (typically 1000-1200pA @ 30 Hz and 10 action potentials every second). **E,F** Box plots of pooled data depicting the minimum number of action potentials required for emergence of BF and its duration under differing frequencies of inducing action potentials (for the box plots, left to right, the n values are 68, 15, 12, 12 and 7, respectively) **G,H.** Single example waveforms and corresponding phase plots of spikelets nested within full spikes (the latter defined as those overshooting 0 mV) observed during BF episodes in a single mouse and human NGFC. Black and orange data represent that derived mouse and human NGFCS, respectively.

Figure 2. Short-term potentiation of somatic-depolarization driven excitability (STP-SE) in mouse and human NGFCs after cessation of BF. A. Single example voltage traces in response to increasing square wave somatic depolarizing current injections before and after induction of BF. Values under each pair of traces (Pre-BF and Post-BF) indicates the size of the 1 second duration current injection. **B.** Pooled data input/output curves of action potential number in response to increasing amplitudes of depolarizing current injections (50pA – 220pA; 25 pA increments; n=12 and 3 for mouse and human NGFCs, respectively). **C.** Line plots of AP output before and after BF (calculated as the total sum of APs in response to all current injection steps) in individual mouse (n=12; paired t-test; p= 0.0000083) and human NGFCs (n=3; paired t-test; p= 0.012) tested . **D.** Single example current traces from NGFCs in response to depolarizing voltage steps (magnitude of steps from a holding potential of -70mV are indicated under each pair of traces) showing action current output before and after BF. **E.** Pooled data showing input/output curves depicting number of action currents in response to depolarizing voltage steps (5 mV to 30 mV; 5 mV increments) before and after BF induction (n= 5 and 3 for mouse and human NGFCs, respectively). **F.** Single example time course of action current output in response to 25 mV depolarizing voltage steps (sweep interval 10s) under baseline conditions and after BF induction. **G.** Box plots depicting the duration of increased action current output to 25 mV depolarizing voltage steps after a single BF episode (post-BF1) and after 4 BF episodes (post BF-4) in mouse (n=11 and 4 for mouse and human NGFCs, respectively; paired t-test, p = 0.007)

Figure 3. STP-SE in mouse and human NGFCs occurs in the absence of BF

A-C. Single example time course of the conditioning protocol employed to elicit STP-SE in mouse and human NGFCs. Action potential output was elicited to a test rheobase depolarizing current injection (300 ms; typically 100pA - 140pA; baseline) in the absence (baseline) and during conditioning action potentials (induction; 10 depolarizing steps of 2 ms width; 1000pA - 1200pA). Conditioning action potentials were terminated upon visualization of a marked loss in 1st spike latency (doted vertical lines) invariably accompanied by increased action potential output in response to the test depolarizing current injection (post-induction). **D.** Pooled time course of action potential output (measured as number of action potentials in response to the test rheobase current injection) during the entire STP-SE induction protocol. Vertical dotted line indicates the commencement of induction with its termination occurring at varying times for each tested cell. Time course plots are from mouse (black) and human (orange) NGFCs displaying STP-SE (n = 9 and 4 for mouse and human NGFCs, respectively). For NGFCs (n = 7 and 2 for mouse and human, respectively) and non-NGFCs (n = 4 and 3 for mouse and human non-NGFCs, respectively) that did not show STP-SE data were pooled (dashed black and orange) between species. **E.** Box plots comparing number of conditioning action potentials required for BF (note these data are replotted from Figure 1E; n = 68 and 12, for mouse and human NGFCS, respectively) and STP-SE (n = 9 and 4, for mouse and human NGFCs, respectively). Paired t-test p-values were 0.0004 and 0.031 for mouse and human, respectively. **F,G**. Phase plots of action potential output to the test depolarizing test pulse during baseline (solid lines) and after induction of STP-SE (dotted lines) in single example mouse and human NGFCs. **H,I.** Line plots demonstrating hyperpolarization of action potential threshold and reduction of spike latency following induction of STP-SE in mouse and human NGFCs. Paired t-test p-values for comparisons of mouse AP threshold and latency (baseline vs. STP-SE) were 0.0000028 and 0.000025, respectively (n = 9). Paired t-test p-values for comparisons of human AP threshold and latency (baseline vs. STP-SE) were 0.000085 and 0.003, respectively (n = 4).

Figure 4. Pharmacological block of a subthreshold transient K^+-conductance mimics the AP latency and threshold modulation seen in STP-SE. A. Single example voltage trace to a depolarizing current injection (120 pA) in the presence of 1μm TTX and 200 μm $NiCl_2$ to block voltage gated Na^+ and

low-threshold activated Ca^{2+} channels, respectively. **B.** Representative voltage-gated outward K^+-currents activated in response to a series of predominantly subthreshold depolarizing voltage steps. Transient (open circle) and sustained (closed circle) components are labeled **C.** Pooled data of the current-voltage curve of outward peak and sustained K^+-currents with gray shaded area depicting the mean action potential threshold measured in NGFCs (n = 6). **D.** Box plot data depicting the pharmacological sensitivity of the subthreshold outward conductance to a subthreshold voltage step (-30 mV) by 100-200nM DTX, 100μm (low 4-AP) and 1-3mM 4-AP (high 4-AP; n = 5, 7 and 11, respectively). p-values for DTX and high 4-AP datasets (Wilcoxin signed rank test) and paired t-test for low 4-AP were 0.44, 0.00098 and 0.02, respectively. **E.** Single trace example of the pharmacological isolation of high 4-AP sensitive subthreshold outward K^+-current elicited in NGFCs characterized by a transient, inactivating time course. **F,G**. Single trace examples showing the effect of DTX and high 4-AP on action potential output upon rheobase current step injections (120pA). **H.** Single trace examples comparing the effect of action potential output to a rheobase current injection performed with K^+-gluconate intracellular solution without (control; left trace) or with added 4-AP (intra-4-AP; right green trace; 3mM). **I.** Pooled data showing a comparison of the effects of DTX (n=10), low 4-AP (n=9), high 4-AP (n=12), intra-4-AP (3mM; n=7) and STP-SE (n=9) on action potential latency and threshold in relation to that seen with STP-SE (n=9).

Figure 5. Functional availability of I_{KA} modulates intrinsic excitability and induction requirements of STP-SE. A. Single trace examples showing the effect of DTX (top traces), high 4-AP (middle traces) and with K^+-gluconate intracellular solution without (control; bottom left trace) versus 4-AP (intra-4-AP; bottom right green trace; 3mM) on action potential output upon 1.5 x threshold current step injections **B.** Pooled data showing the effects of STP-SE (n=8), DTX (100-200nM; n=8), low 4-AP (100μm; n=9), high 4-AP (1mM; n=7) on intrinsic excitability measured the total number of action potentials to a series of depolarizing current injections. p-values from unpaired t-tests comparing increase in intrinsic excitability between STP-SE versus DTX, STP-SE versus low-4AP or STP-SE versus high-4AP = 0.011, 0.045 and 0.38, respectively. **C.** Pooled data comparing intrinsic excitability of NGFCs to series of depolarizing current injections with control intracellular K^+-gluconate (n=7; black trace) or K^+-gluconate with added 4-AP (interleaved experiments; intra 4-AP 3mM; n=7; green trace). **D.** Effect of high 4-AP (1mM) on voltage

response of NGFC to a subthreshold current injection step (120pA). **E.** Single trace examples illustrating recovery of subthreshold I_{KA} current following successive depolarizing voltage steps of the same amplitude (typically 120 pA). **F.** Corresponding action potential output of NGFCs to pairs of temporally separated threshold current injections (200ms) shown previously in (**E**) to result in a range of I_{KA} inactivation. **G.** Pooled data showing comparison between the level of I_{KA} inactivation induced measured as ratio of peak amplitude of I_{KA} (n=6) and ratio of latency (n=6) of the first action potential between the two successive depolarizing voltage/current steps, respectively. **H.** Pooled data showing relationship between the level of I_{KA} inactivation induced (n=6) and increase in action potential output (n=6), the latter measured as percentage increase in number of action potentials of between the two successive depolarizing current steps. **I.** Pooled time course of action potential output (measured as number of action potentials in response to the test rheobase current injection as percentage of baseline) during the entire STP-SE induction protocol in NGFCs with either control intracellular K^+-gluconate (n=7; black plot) or K^+-gluconate with added 4-AP (interleaved experiments; intra 4-AP 3mM; n=7; green plot). Vertical dotted line indicates the commencement of induction with its termination occurring at varying times for each tested cell. **J.** Box plot showing number of conditioning APs required for expression of STP-SE with control or intra-4AP K^+-gluconate solution (interleaved experiments; n=5 for both conditions; unpaired t-test p value = 0.00005).

Figure 6. I_{KA} in NGFCs is predominantly mediated by Kv4-subunit containing channels. A. Uniform Manifold Approximation and Projection (UMAP) plot of RNAseq data publicly available from the Allen Brain Institute (see methods for details) highlighting clusters corresponding to CGE-NGFCs (green; 3626 cells) and hippocampal pyramidal cells (blue; 2530 cells). **B.** Violin plots depicting comparison of mRNA levels in CGE-NGFCs that encode for subunits of I_{KA} channels. Median values are depicted above each plot. **C**. Top, middle; Voltage steps and corresponding single current traces illustrating the protocol employed to isolate I_{KA} and I_{KDR}. Bottom; Single traces illustrating the effects of TEA (2-10 mM) and AmmTx3 (500nM) on the isolated I_{KA} and I_{KDR}. **D.** Box plots depicting inhibition of I_{KA} and I_{KDR} by TEA (n=8) and AmmTx3 (n=4). **E.** Scatterplot of median expression levels of KCND2 versus KCND3 mRNA in CGE-NGFCs and hippocampal pyramidal cells. **F.** Representative confocal images of KCND2 and

KCND3 transcript expression in CA1 pyramidal cells revealed by RNAscope (see methods for details; scale bar = 100μm) **G.** Representative confocal image of the distribution of putative NGFCs (via expression of NDNF mRNA transcripts) in CA1 SLM (scale bar -= 100μM). **H,I.** Representative confocal images of mRNA expression of *KCND2* and *KNCD3* in putative NGFCs (NDNF-expressing) in CA1 SLM. (Scale bars = 50μm for top panels; 20μm for bottom panels) **J.** Split-violin plots depicting comparison in the expression levels of mRNA transcripts encoding known auxiliary subunits of Kv4-containing channels (KCHIPs and DPLPs) in CGE-NGFCs (green) versus hippocampal pyramidal cells (blue).

Figure 7. STP-SE manifests as an increase in afferent recruitment of NGFCS via enhanced E-S coupling. A. Single traces showing the effect of AmmTx3 (500 nM) on EPSC (top traces) and corresponding EPSP (bottom trace) in a given hippocampal NGFC in response to electrical stimulation of SLM afferent fibers (2 x 30Hz). **B.** Box plots of EPSC amplitudes (EPSC1 versus EPSC2) under baseline conditions and after AmmTx3 treatment (n=7; p values for EPSC1 and EPSC2 comparisons are 0.11 and 0.27, respectively). **C.** Box plots of paired pulse ratio (EPSC2 peak amplitude/EPSC1 peak amplitude) under baseline conditions and after AmmTx3 treatment (n=7; p value = 0.36). **D.** Box plots of EPSP summation measured as absolute Vm at peak of EPSP1 and EPSP2 under baseline conditions and after AmmTx3 treatment (n=7; =7; p values for EPSP1 and EPSP2 comparisons are 0.005 and 0.016, respectively)). **E-G.** Single trace examples depicting a time course of E-S coupling (SLM afferent stimulation delivered at 5 X 30 Hz) during baseline conditions and after STP-SE induction. **H.** Line plot depicting increased E-S coupling measured as spike probability during 10 sweeps of baseline versus 10 sweeps immediately after STP-SE induction (n=9; p value = 0.002). **I.** Box plot illustrating duration of enhanced E-S coupling following STP-SE induction (n=9).

Supplementary Figure 1. Privileged induction of barrage firing in mouse and human NGFCs. A, B. Confocal mages of biocytin filled cortico-hippocampal NGFCs and non-NGFCs in *stratum lacunosum-moleculare* (SLM) and Layer I. Insets show firing patterns of non-NGFCs to suprathreshold current injections. Note: reconstructed drawings and corresponding firing patterns of NGFCs are depicted in main Figure 1A, B. **C.** Histogram showing the prevalence in the ability to induce BF in mouse (black; n=124)

and human (orange; n=25) NGFCs. **D.** Histogram showing the inability to induce BF in mouse (black; n=26) and human (orange; n=33) non-NGFCs.

Supplementary Figure 2. Induction of multiple barrage firing episodes in individual mouse and human NGFCs. A. Single trace example showing the inability to elicit prolonged BF episodes in single NGFC following immediate continuation of the induction protocol (30 X 10Hz induction; see main Figure 1 for details of induction). **B.** Single trace showing repeated BF can by induced in a given NGFC following a determined elapsed period which in this example is 4.4 minutes. **C.** Individual data plot showing the relationship between the duration of the inter-induction period and failure/success of eliciting a second BF episode (n=61). **D.** Line plots showing duration of BF for multiple subsequent BF episodes (BF1 thru BF4) in any given mouse or human NGFC. Plotted as combined mean for BF1,BF2 and BF3,BF4 (n=16 and 6 for mouse and human NGFCs, respectively). **E**. Corresponding box plots of the % change in the duration of BF elicited in any given NGFC induced by subsequent BF induction protocols (4 induction protocols in each NGFC were delivered with inter induction interval greater than 1 minute). Data are expressed as a percentage change in these parameters for the mean of BF3,BF4 versus the mean of BF1, BF2 in each NGFC tested (n=16 and 6 for mouse and human NGFCs, respectively). Paired t-test p values = 0.0077 and 0.162 for mouse and human NGFCs, respectively).

Supplementary Figure 3. Inability to induce STP-SE in a subpopulation of NGFCs and all non-NGFCs tested. A-D Time course traces demonstrating the inability of a single example mouse NGFC and non-NGFC to express STP-SE. Traces in B and D are magnified for clarity at the time points in the induction protocol as indicated.

Supplementary Figure 4. Delineation of mouse cortico-hippocampal cell clusters obtained from publicly available Allen Brain Institute scRNAseq data. A. Uniform Manifold Approximation and Projection (UMAP) dimension reductionality of ~76,000 single-cell transcriptomes, depicting the clustering of broad cell types. **B.** Clustering of CGE and MGE-derived GABAergic interneuron subtypes. Cell clusters were colored and annotated post hoc based on their transcriptional profile identities (see

methods). **C.** Violin plots showing the distribution of expression levels of established cell type-enriched marker genes across GABAergic interneuron subtypes (see methods). Boxed regions illustrate the CGE-NGFCs (3626 cells) and hippocampal pyramidal cell (2530 cells) clusters delineated via the combined expression of the specific genes highlighted (see methods).

Supplementary Figure 5. E-S coupling potentiation not attributed to modulation of spontaneous EPSC parameters. A. Traces showing spontaneous AMPA-receptor mediated EPSCs (top) under baseline conditions (gray) and immediately after cessation of a 4th BF episode (post-BF4; black) elicited in a given NGFC. Bottom trace shows overlaid ensemble average of AMPA-receptor mediated EPSCs during baseline and after 4th BF episode. **B,C,D.** Box plots of AMPA-receptor mediated sEPSC amplitude, frequency and decay time constant measured under baseline (n=6) and immediately following cessation of BF, BF2 ,BF3 and BF4 (n=6) episodes. Paired t-test for comparison of sEPSC amplitude, frequency and tau decay between post-BF1 versus post-BF4 were 0.02, 0.64 and 0.95, respectively.

Supplementary Figure 6. Comparison of subthreshold Kv1 and Kv4 subunit gene expression between mouse and human NGFCs and other IN subtypes. A,B. mRNA expression levels of *Kcna1, Kcnd2 and Kcnd3* in neural cell types. Data are from publicly available resources from the Allen Brain Institute (https://portal.brain-map.org/) and the McCarroll Laboratory, Harvard Medical School (http://interneuron.mccarrolllab.org/). Green shaded box in **A** denotes the cluster corresponding to human cortical NGFCs. ID2+ cells in **B** corresponds to a subpopulation of human cortical NGFCs.

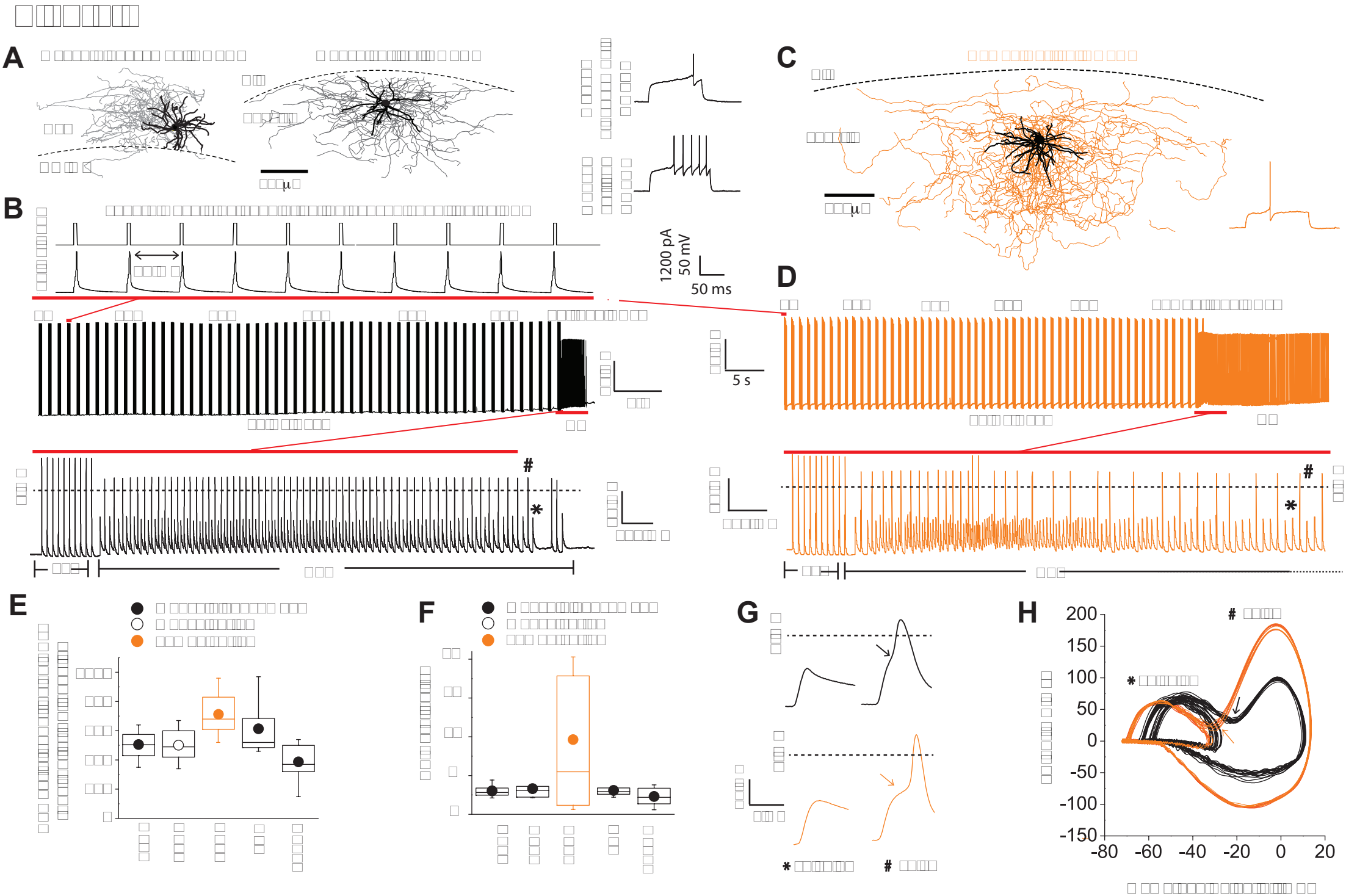
A
B
C
D
E
F
G
H
1200 pA
50 mV
50 ms
5 s
#
*
200
150
100
50
0
-50
-100
-150
-80
-60
-40
-20
0
20

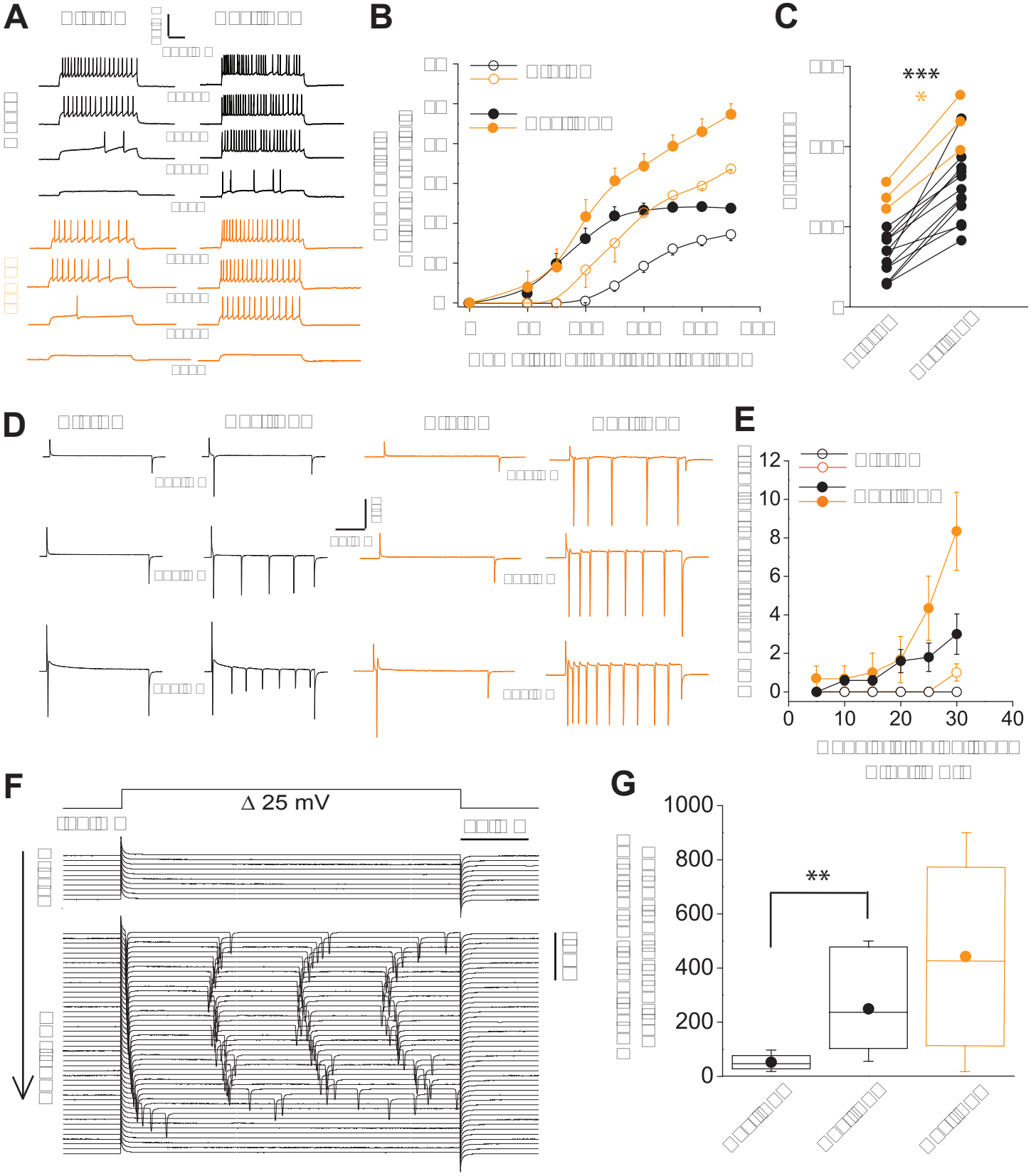
A
B
C
***
*
D
E
12
10
8
6
4
2
0
0
10
20
30
40
F
Δ 25 mV
G
1000
800
600
400
200
0
**

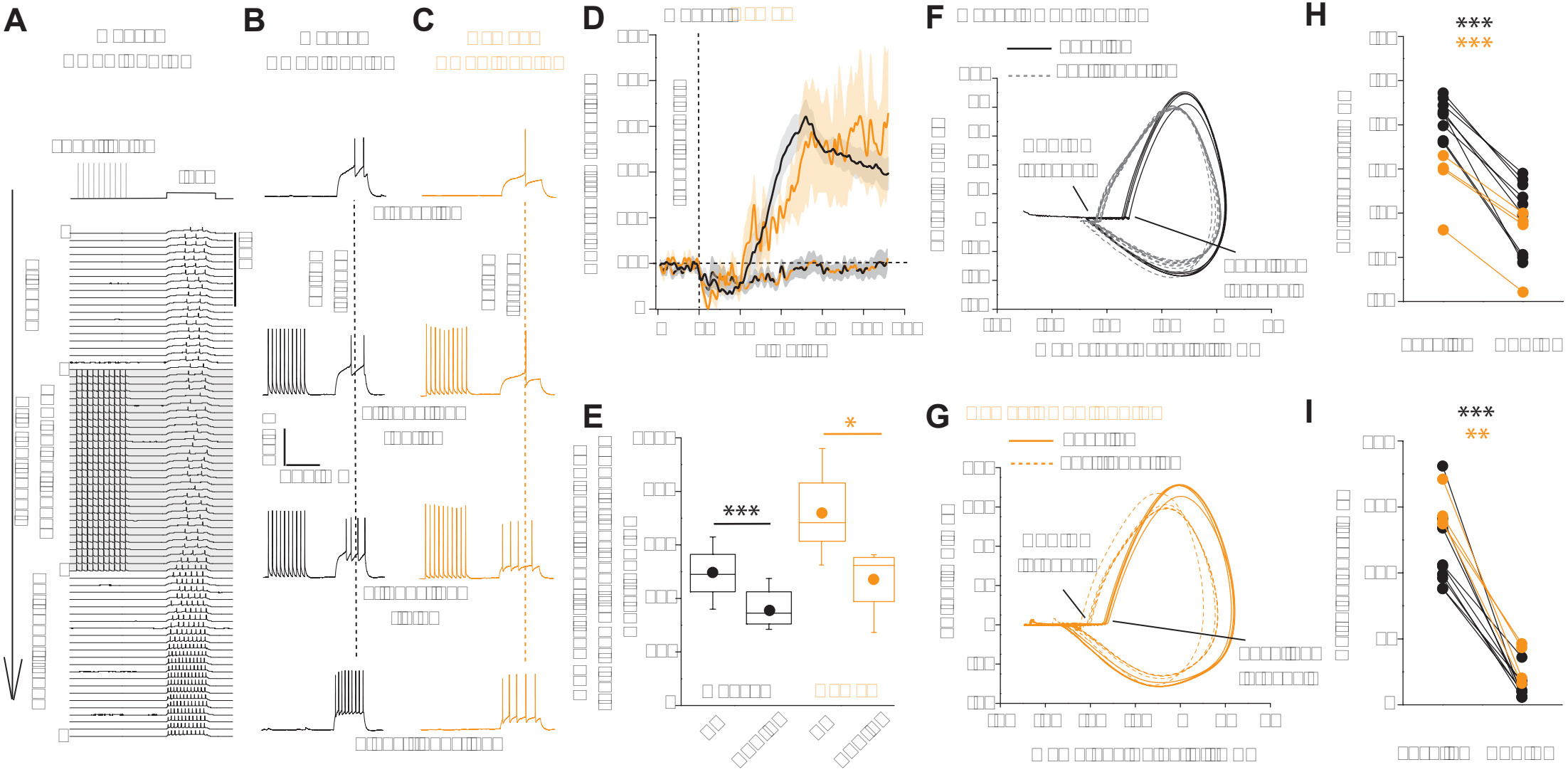
A
B
C
D
E
F
G
H
I
***
*
**

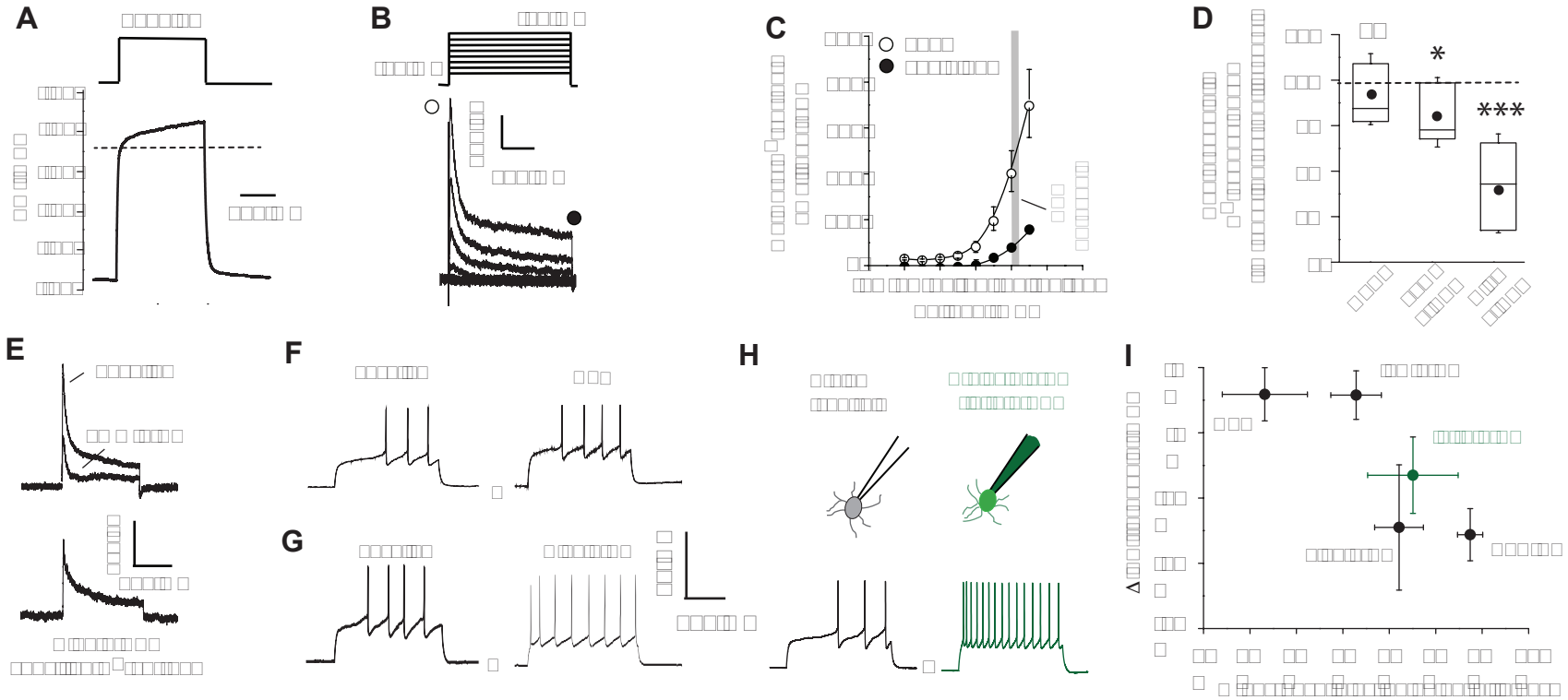
A
B
C
D
E
F
G
H
I
*
***

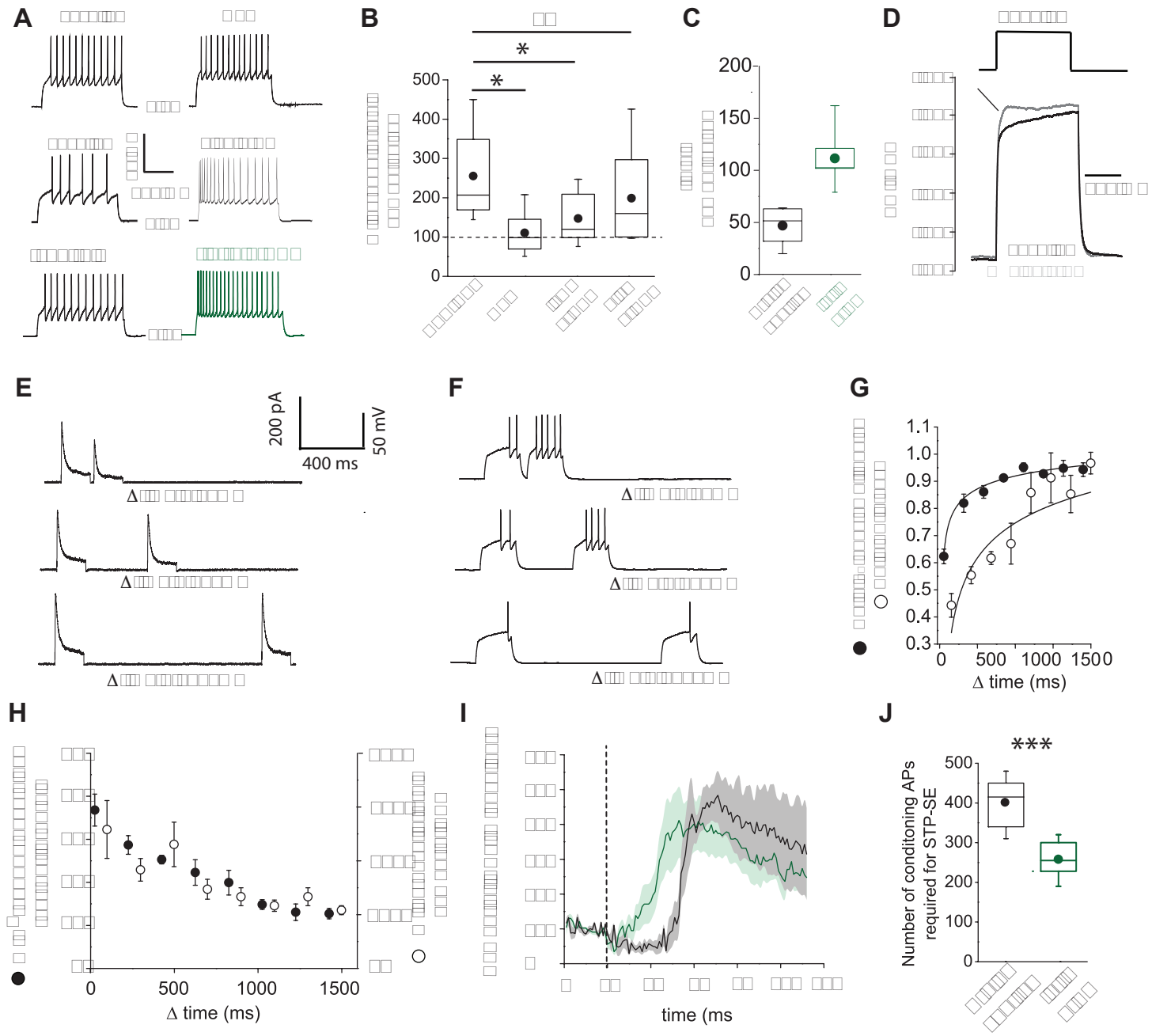
A
B
C
D
E
200 pA
50 mV
400 ms
F
G
1.1
1.0
0.9
0.8
0.7
0.6
0.5
0.4
0.3
0
500
1000
1500
Δ time (ms)
H
Δ time (ms)
I
time (ms
J
***
Number of conditoning APs required for STP-SE
500
400
300
200
100
0

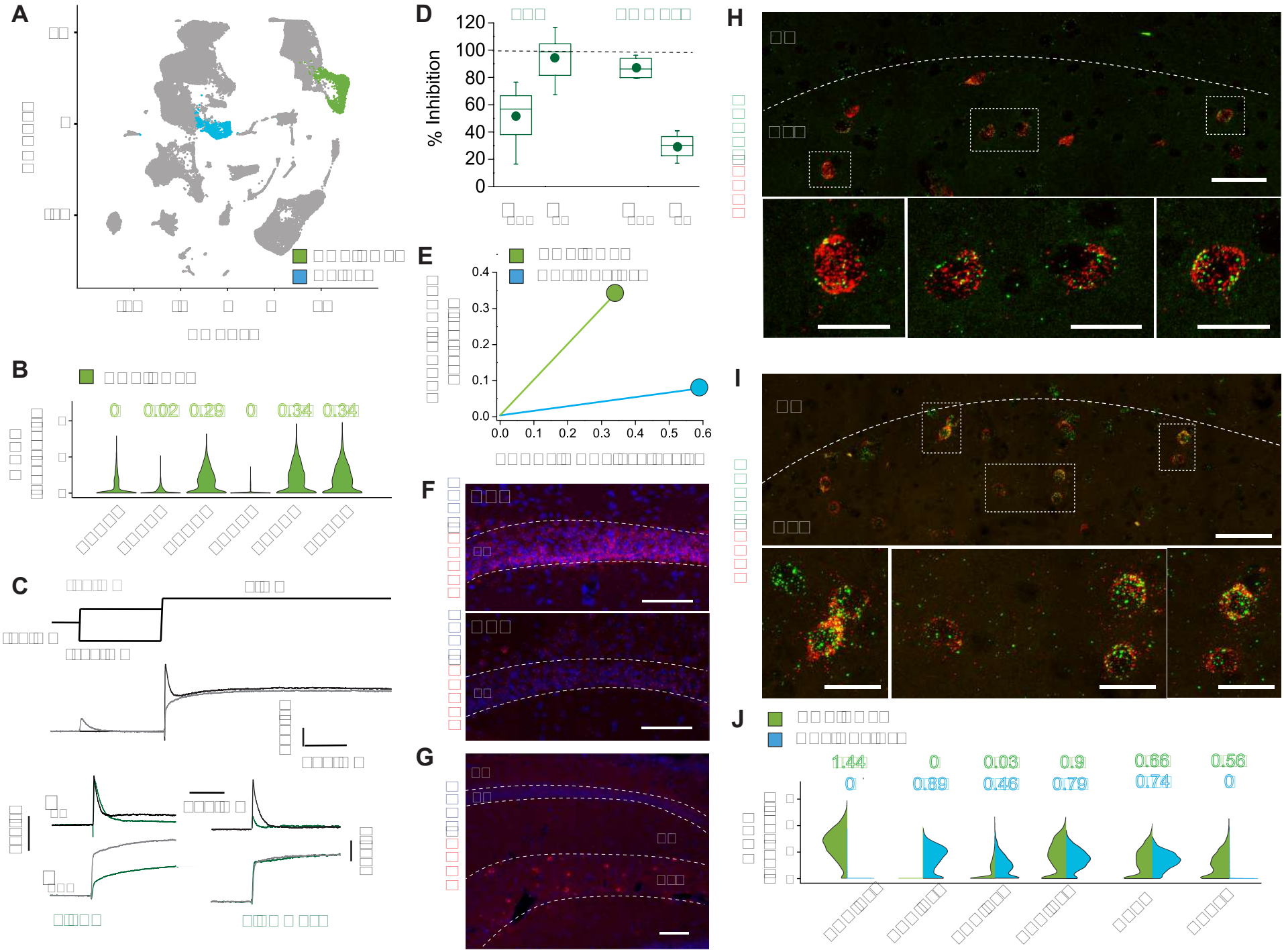
A
B
C
D
% Inhibition
120
100
80
60
40
20
0
E
0.4
0.3
0.2
0.1
0.0
0.0
0.1
0.2
0.3
0.4
0.5
0.6
F
G
H
I
J
0
0.02
0.29
0
0.34
0.34
1.44
0
0.03
0.9
0.66
0.56
0
0.89
0.46
0.79
0.74
0

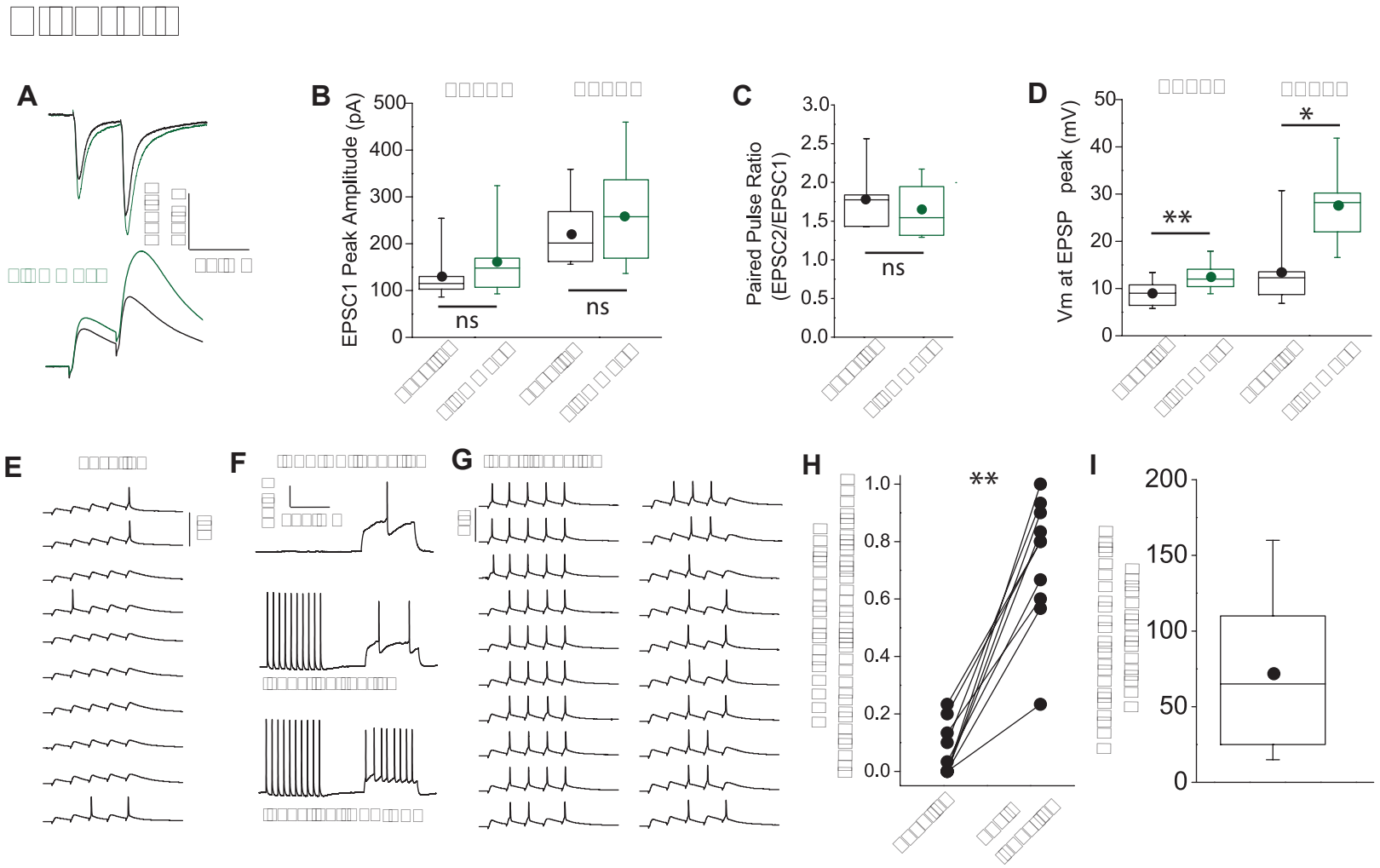
A
B
EPSC1 Peak Amplitude (pA)
500
400
300
200
100
0
ns
ns
C
Paired Pulse Ratio
(EPSC2/EPSC1)
3.0
2.5
2.0
1.5
1.0
0.5
0.0
ns
D
Vm at EPSP peak (mV)
50
40
30
20
10
0
**
*
E
F
G
H
1.0
0.8
0.6
0.4
0.2
0.0
**
I
200
150
100
50
0

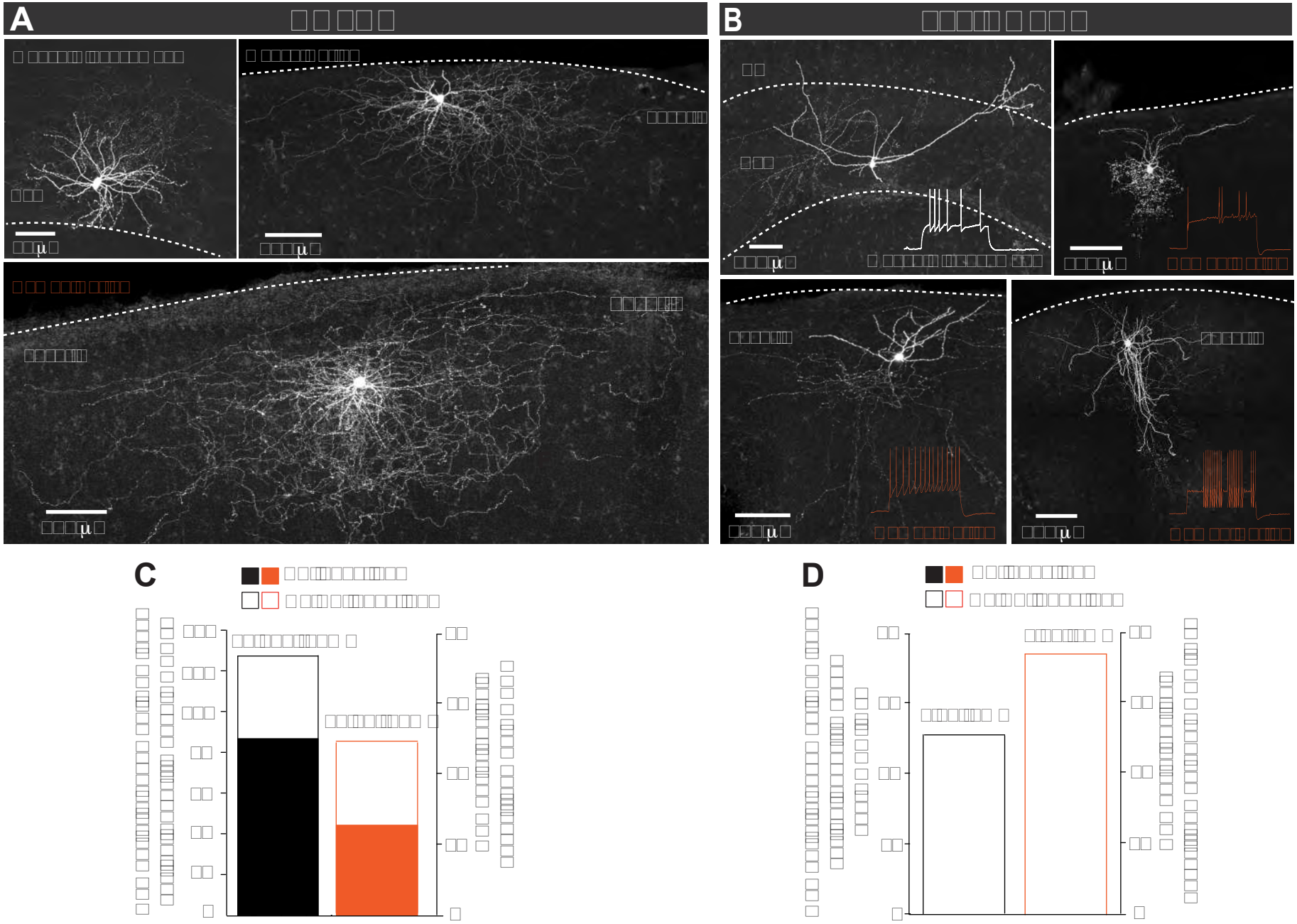
A
B
C
D

Supplementary Figure 2

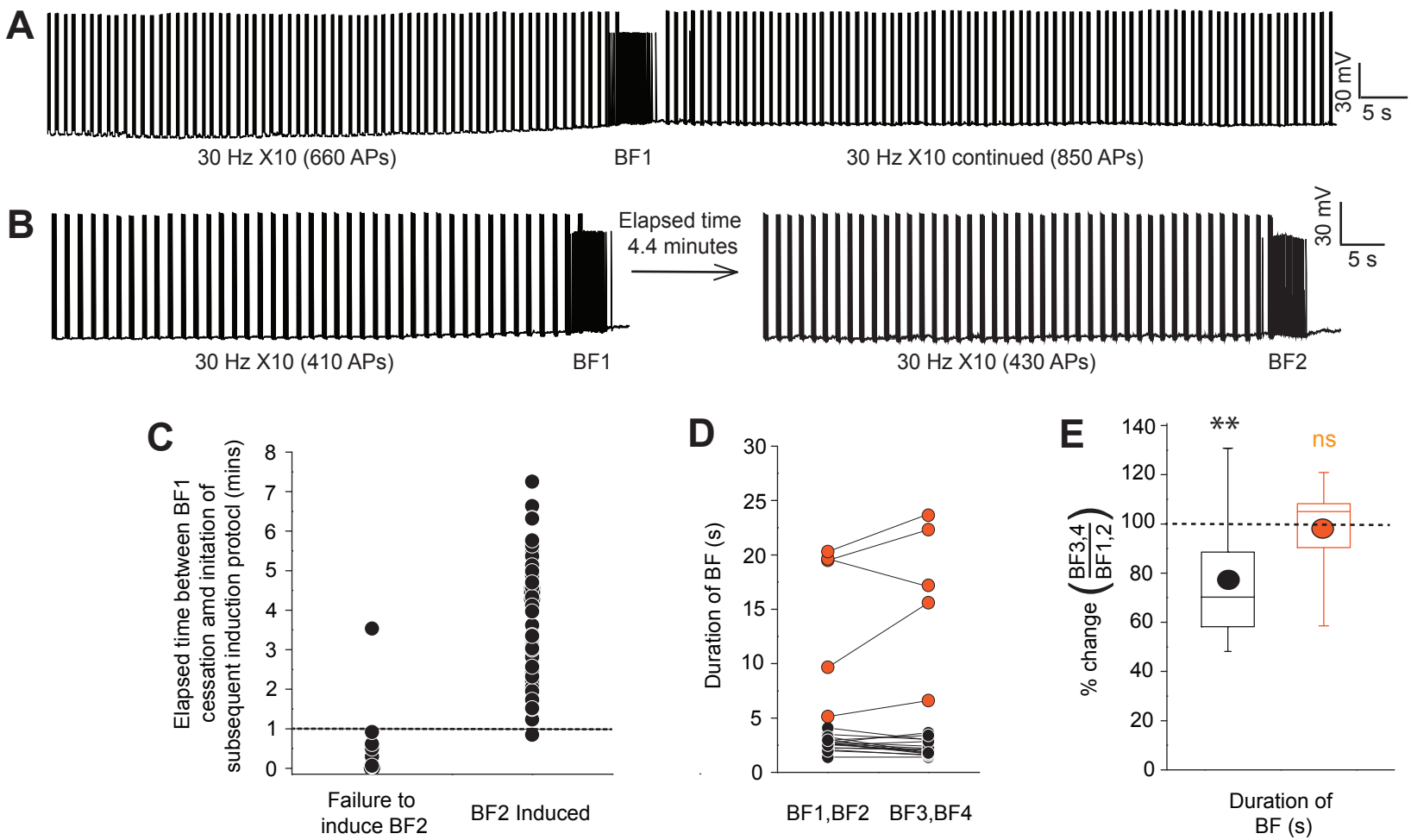

Supplementary Figure 3

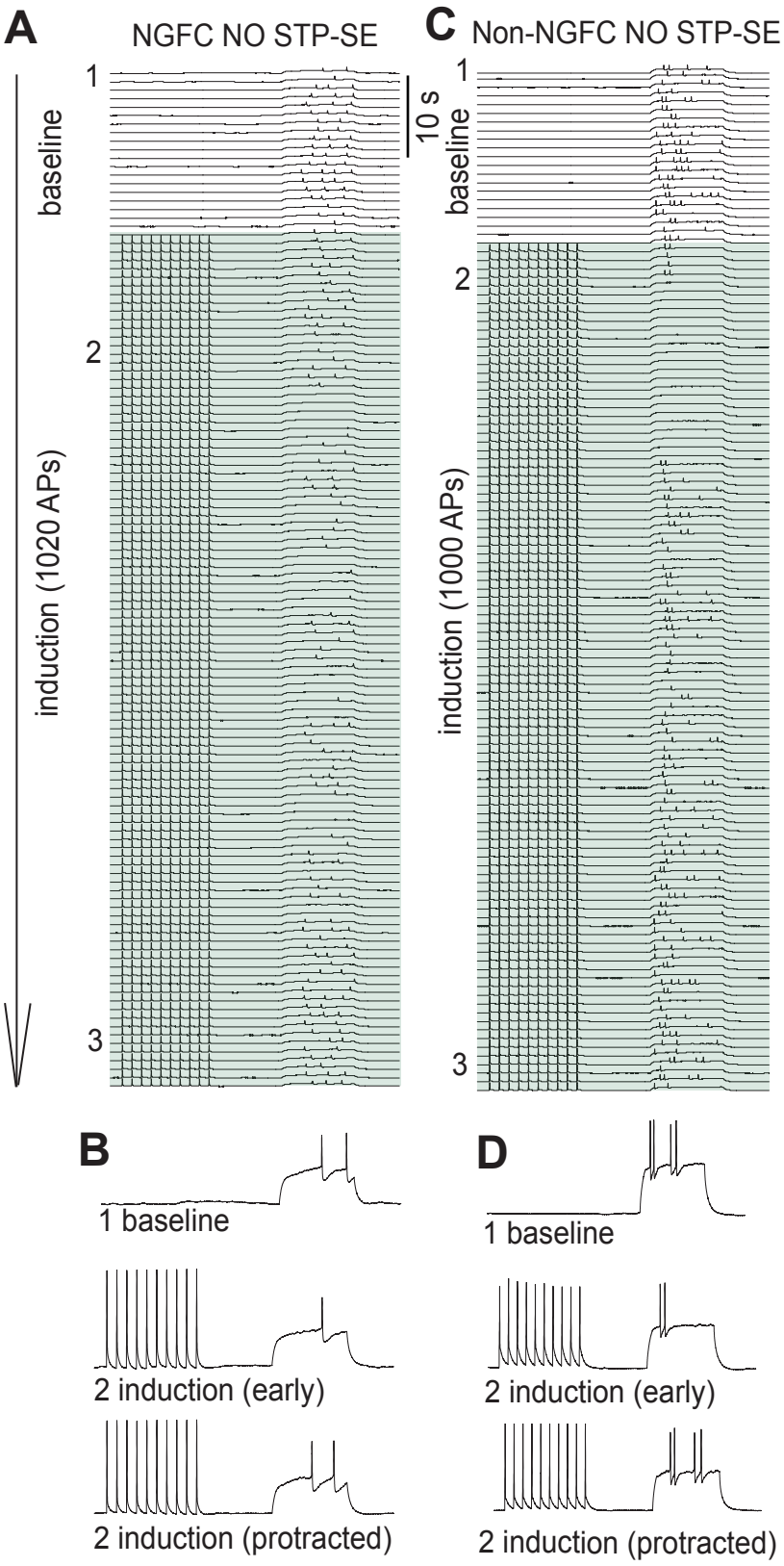

Supplementary Figure 4

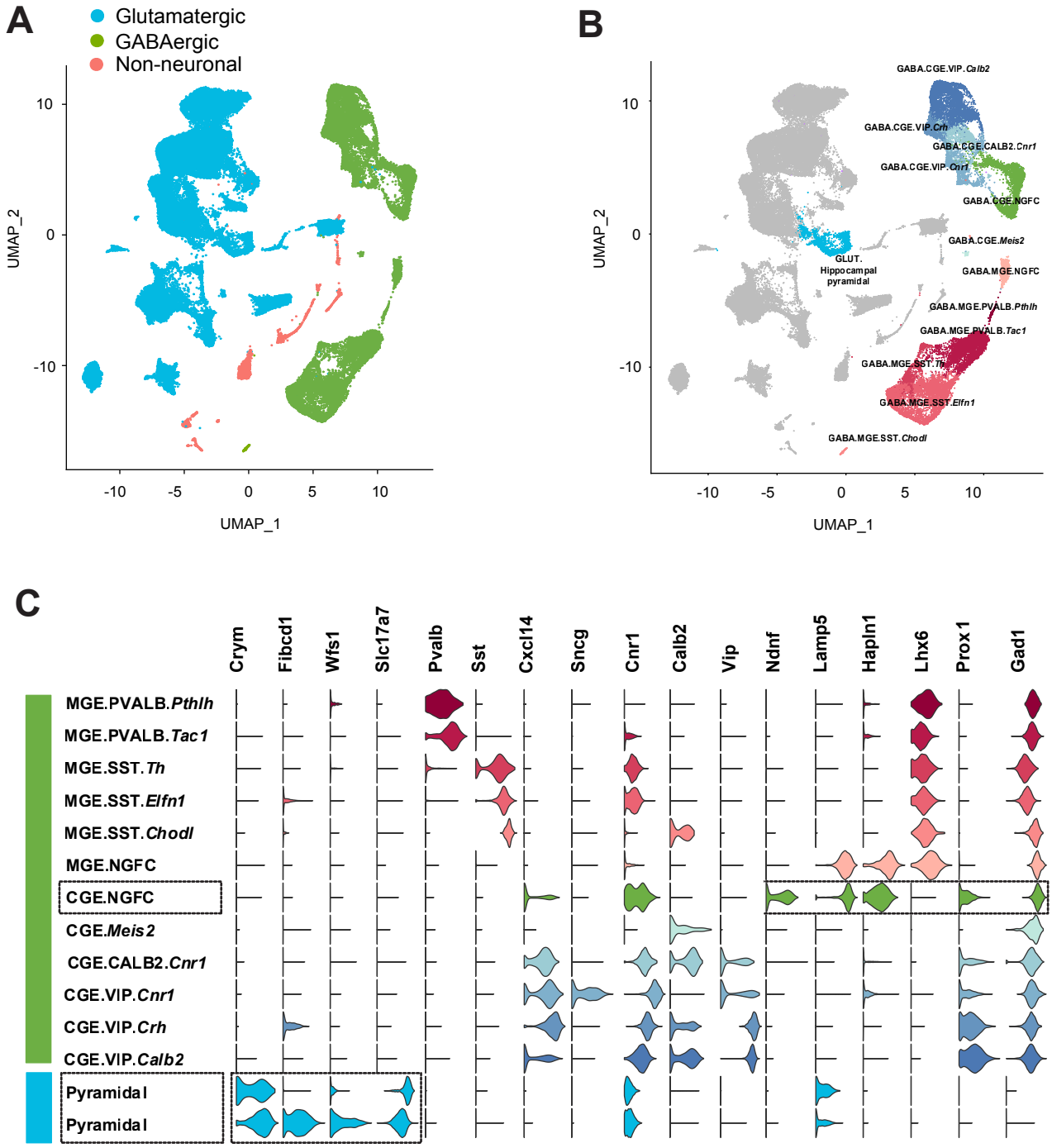

Supplementary Figure 5

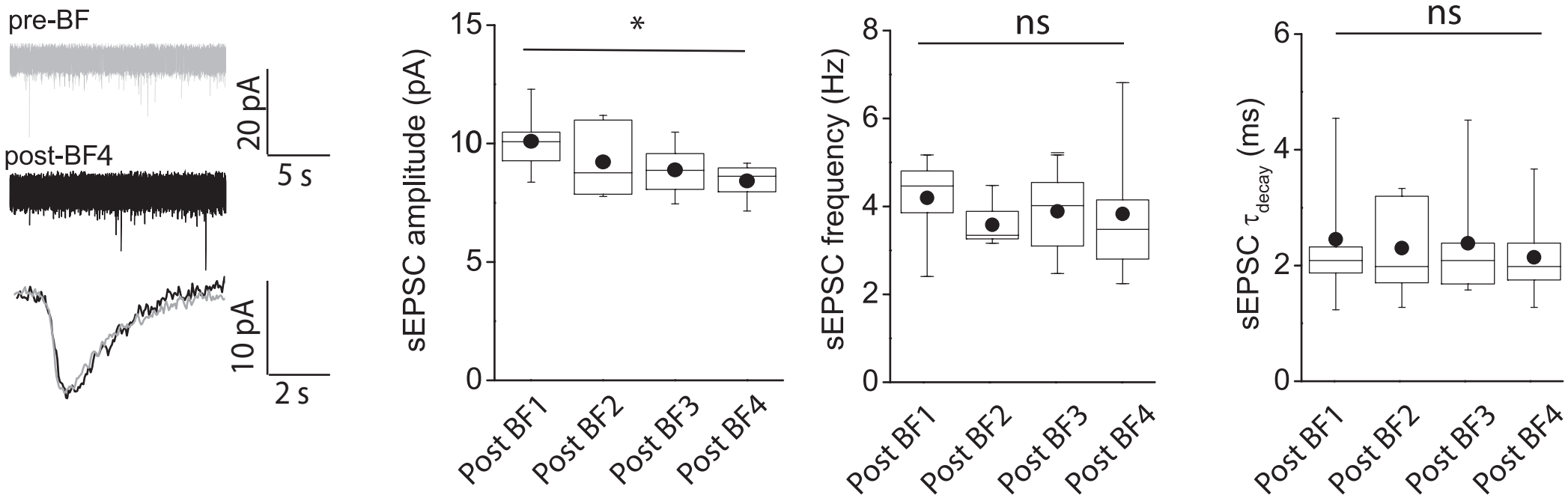

Supplementary Figure 6

https://portal.brain-map.org/

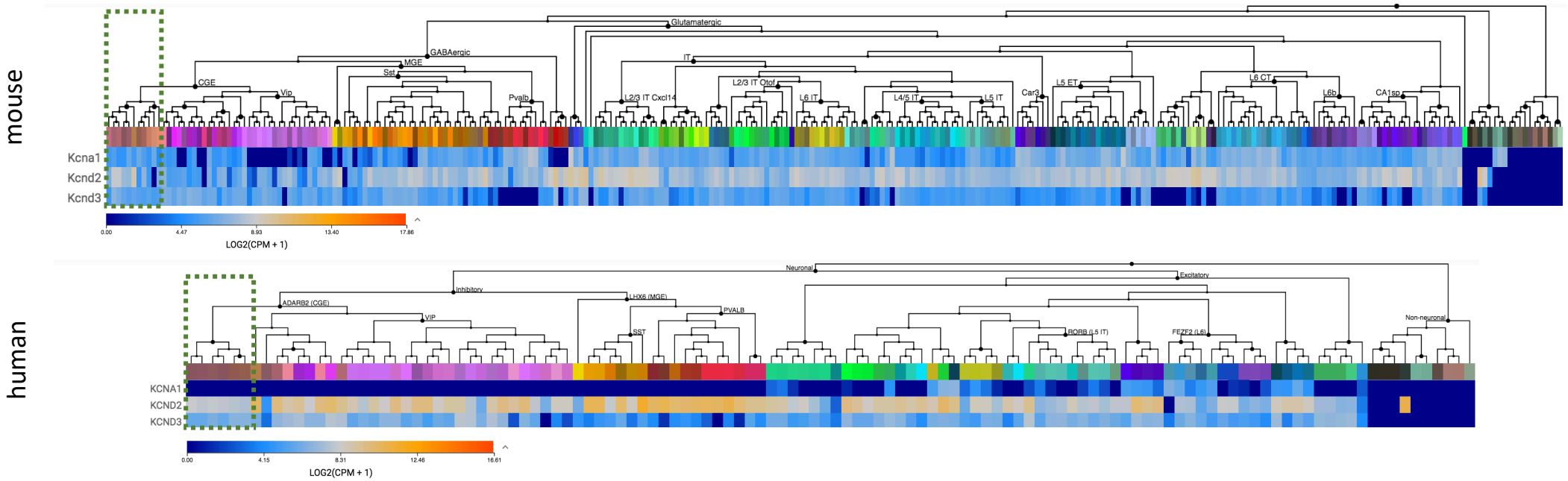
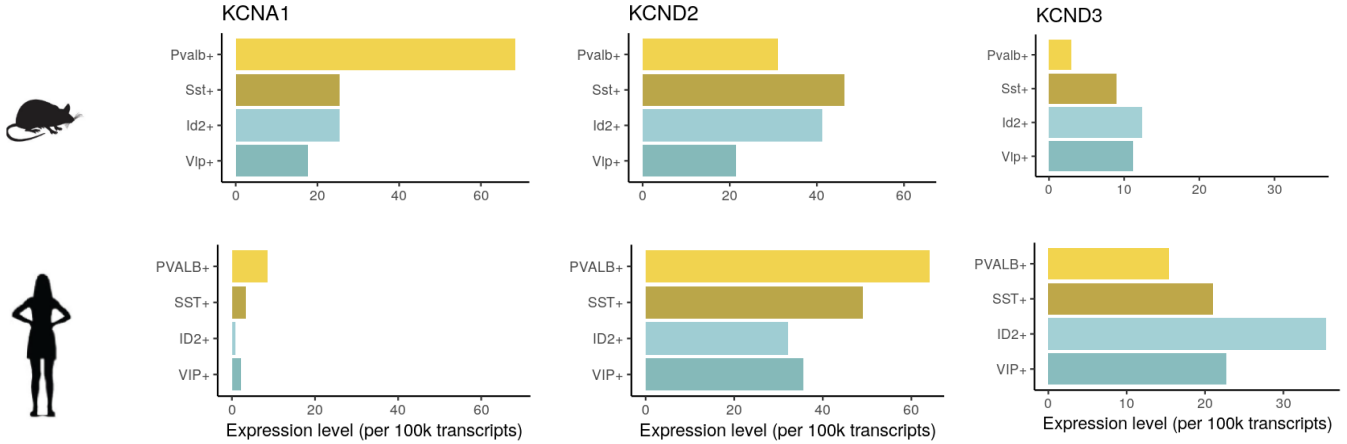
http://interneuron.mccarrolllab.org/